AD-A150 819 FRACTURE BEHAVIOR OF CERAMIC COMPOSITES(U) MATERIALS SCIENCES CORP SPRING HOUSE PA K W BUESKING ET AL. AUG 83 MSC/TFR/1402/1503 AFOSR-TR-85-0044 1/1

UNCLASSIFIED F49620-82-C-0041 F/G 11/2 NL

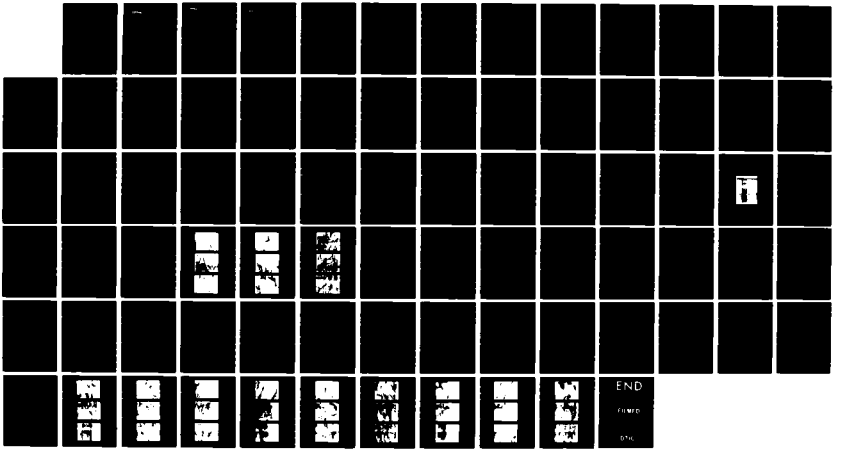

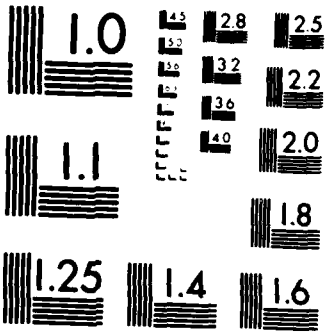

MICROCOPY RESOLUTION TEST CHART
NATIONAL BUREAU OF STANDARDS 1963 A

AFOSR-TR- 85-0044

(2)

Materials Sciences Corporation

AD-A150 819

FRACTURE BEHAVIOR

OF CERAMIC COMPOSITES

K. W. BUESKING AND S. N. CHATTERJEE

The views and conclusions contained in this document are those of the author and should not be interpreted as necessarily representing the official policies or endorsements, either expressed or implied, of the Air Force Office of Scientific Research of the U.S. Government.

DTIC
ELECTE
MAR 0 1 1985
E

DTIC FILE COPY

AIR FORCE OFFICE OF SCIENTIFIC RESEARCH
Bolling Air Force Base, DC

MSC TFR 1402/1503
August, 1983

Approved for public release;
distribution unlimited.

85 02 13 057

Materials Sciences Corporation

FRACTURE BEHAVIOR

OF CERAMIC COMPOSITES

Technical Final Report
MSC TFR 1402/1503
August, 1983

Prepared by:

K. W. Buesking and S. N. Chatterjee

Prepared for:

Air Force Office of Scientific Research
Bolling Air Force Base, DC

AIR FORCE OFFICE OF SCIENTIFIC RESEARCH (AFSC)
NOTICE OF TRANSMITTAL TO DTIC
This technical report has been reviewed and is approved for public release IAW AFR 190-12.
Distribution is unlimited.
MATTHEW J. KEMPER
Chief, Technical Information Division

Gwynedd Plaza II, Bethlehem Pike, Spring House, PA • 215-542-8400

UNCLASSIFIED
SECURITY CLASSIFICATION OF THIS PAGE (When Data Entered)

REPORT DOCUMENTATION PAGE		READ INSTRUCTIONS BEFORE COMPLETING FORM
1. REPORT NUMBER AFOSR-TR-85-0044	2. GOVT ACCESSION NO.	3. RECIPIENT'S CATALOG NUMBER
4. TITLE (and Subtitle) FRACTURE BEHAVIOR OF CERAMIC COMPOSITES		5. TYPE OF REPORT & PERIOD COVERED Final Report 4/1/82 to 7/31/83
		6. PERFORMING ORG. REPORT NUMBER
7. AUTHOR(s) K. W. Buesking S. N. Chatterjee		8. CONTRACT OR GRANT NUMBER(s) F49620-82-C-0041
9. PERFORMING ORGANIZATION NAME AND ADDRESS Materials Sciences Corporation Gwynedd Plaza II, Bethlehem Pike Spring House, PA 19477		10. PROGRAM ELEMENT, PROJECT, TASK AREA & WORK UNIT NUMBERS 61102F 2307/B2
11. CONTROLLING OFFICE NAME AND ADDRESS Air Force Office of Scientific Research NA Building 410 Bolling AFB, DC 20332-6448		12. REPORT DATE August, 1983
		13. NUMBER OF PAGES 77
14. MONITORING AGENCY NAME & ADDRESS (if different from Controlling Office)		15. SECURITY CLASS. (of this report) Unclassified
		15a. DECLASSIFICATION DOWNGRADING SCHEDULE

16. DISTRIBUTION STATEMENT (of this Report)

Approved for public release, distribution unlimited

17. DISTRIBUTION STATEMENT (of the abstract entered in Block 20, if different from Report)

18. SUPPLEMENTARY NOTES

19. KEY WORDS (Continue on reverse side if necessary and identify by block number)

Ceramic Matrix Composites
Flexural Strength
Fracture Toughness
Al_2O_3
SiC Whiskers

20. ABSTRACT (Continue on reverse side if necessary and identify by block number)

A combined experimental and analytical study is described which investigated the strength and fracture toughness of whisker reinforced ceramics. Experiments were performed on Al_2O_3 reinforced with SiC whiskers mechanically loaded in four-point flexure. The results showed an increase in flexural strength and K_{IC} as the whisker content of the composites was increased. Several fracture and strength theories were compared to the experimental results. The hypothesis which appeared most consistent with the

DD FORM 1 JAN 73 1473 EDITION OF 1 NOV 65 IS OBSOLETE -i- UNCLASSIFIED

SECURITY CLASSIFICATION OF THIS PAGE (When Data Entered)

20. (Cont'd.)

data treated the composites as though they contained inherent flaws which were the length of the mean free path between reinforcing whiskers. Using this crack size, the measured flexural strength of the composites could be predicted by applying linear elastic fracture mechanics.

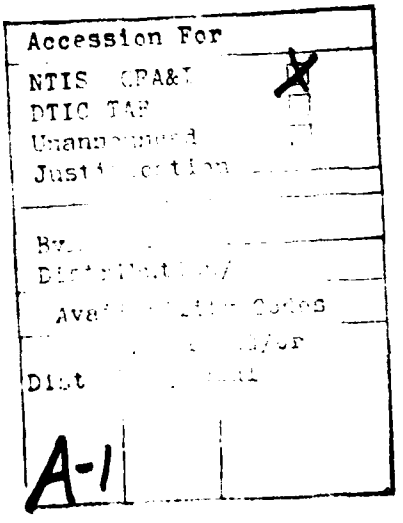

PREFACE

This report presents the results of a study performed under Air Force Office of Scientific Research (AFOSR) contract number F49620-82-C-0041 during the period 1 April 1982 to 31 July 1983. This work was funded under the Department of Defense Small Business Innovative Research program. Mr. Kent Buesking served as the principal investigator and program manager for Materials Sciences Corporation. The ceramic composites were fabricated by Arco-Silag under the direction of Mr. Ronald Beatty. The experiments were performed at Rutgers University and were directed by Drs. Roger Cannon and Steven Danforth. Major David Glasgow served as the AFOSR technical monitor.

APPROVED BY:

Kent W. Buesking

Kent W. Buesking
Program Manager

TABLE OF CONTENTS

INTRODUCTION

This report details the results of a study that was performed under the Department of Defense Small Business and Innovative Research program and addressed the topic of conservation of resources and substitute material technology. The availability of raw materials and natural resources is vital to this nation's economy and security. Depletion of domestic reserves and world political instabilities have pushed this concern to the forefront of present material utilization and future material planning. A major thrust of the recent research has been the investigation of replacing scarce or strategically important materials with alternates that are readily available domestically, reference 1.

High temperature gas turbine materials are a specific application that warrant immediate investigation. Present day turbine materials are metal alloys which contain significant amounts of chromium, cobalt and other materials which are largely imported from unfriendly or unstable countries. The strategic importance of gas turbine materials is obvious, but scarcities in required materials will also affect the domestic economy through increased costs for commercial aircraft and related transportation. Considerable research is already underway to investigate alternate materials for turbine applications, reference 2. Investigations are focusing on such diverse materials as metal superalloys, metal-matrix composites, and directionally solidified metals and ceramics. Of these concepts, the biggest payoffs appear to be associated with ceramics. Ceramics can be low cost, low density, and high strength-to-density ratio materials. Furthermore, ceramics are capable of withstanding temperatures up to 2500F, whereas most metals are limited to thermal environments below 2000F. Higher combustion temperatures imply improved performance, higher engine efficiency, and reduced fuel consumption.

The major drawbacks to bulk ceramics is their brittle behavior and relatively low fracture toughness. The toughness may be improved through the use of fiber-reinforced ceramics. A typical ex-

ample of a fiber-reinforced ceramic is randomly oriented SiC whiskers in a Al_2O_3 matrix. In general, fiber-reinforced materials have excellent fracture toughness when compared to unreinforced bulk materials. For example, the addition of chopped random glass fibers to a polymeric matrix increases the fracture toughness of the matrix by more than two orders of magnitude, reference 3. This is due to two physical phenomena. First, the fibers add their inherent stiffness and strength to the matrix, thereby increasing the composite material fracture toughness. In addition, the fibers also act as crack arrestors. That is, they inhibit the growth of cracks by forcing a propagating crack to change direction, thereby requiring additional energy. These two physical phenomena will also apply to fiber-reinforced ceramics. Thus, there is significant potential for improving the fracture toughness of ceramic turbine blades by fiber reinforcement.

The objective of this program was to define a realistic fracture model for a whisker reinforced ceramic. Considerable work has already been done on failure mechanisms and fracture theory in composites materials. Whisker reinforced ceramics, however, lead to specialized problem areas because of the brittle nature of the matrix, the relatively small ℓ/d ratio of the fibers, and the random arrangement of the fibers. The purpose of this study was to draw upon the considerable work that presently exists in composites fracture theory to define a specialized fracture behavior model that realistically portrays a whisker reinforced ceramic. This will lead to increased applicability of ceramics as high temperature structural materials. Therefore components that are presently fabricated from scarce, costly metals can be replaced with similar structures manufactured from readily available ceramics.

Hopefully, the results of this study will lead to benefits on two distinct levels. On the first level, or most practical level, the program has identified whisker reinforced ceramic material that has potential for high temperature structural appli-

cations. Ceramics are low cost and domestically available, so the problem of materials availability can be alleviated. The high temperature capabilities of the ceramic will also lead to increased combustion temperatures and improved engine performance.

On a more scientific level, the theoretical models investigated in this program can improve the understanding of fracture in whisker reinforced ceramics. The models have been evaluated as material design tools. Although the initial objective was to analyze whisker reinforced ceramics, it is hoped that the model will also be viable for analyzing the fracture of other randomly oriented whisker reinforced composites. Thus, the models may be applied to other types of composites to predict fracture toughness and improve material designs. The potential lies in more efficient and effective uses of composite materials.

OBJECTIVES

The specific goals of this program were the definition of the fracture behavior of a whisker reinforced ceramic, and the identification of the most useful analytic approach for predicting the failure behavior. This study contained tasks concerned with fabricating and testing materials along with an evaluation of the available composite material failure theories.

The first objective was to define the exact fracture mechanism of a fiber-reinforced ceramic. Specifically, this task was designed to answer questions such as: Is the failure fiber dominated, matrix dominated, or a combination? Does the crack exhibit stable propagation before failure? Is the measured fracture toughness of a whisker reinforced ceramic significantly greater than that of a bulk ceramic? Is there any evidence of internal damage to the test specimen before the visible crack begins to propagate?

The second objective was to choose or define an analysis method that was capable of modeling the observed fracture behavior. The method was chosen so that it was able to qualitatively and quantitatively predict the experimental data. The model was also selected to be a useful tool that could be employed to design materials. Therefore, the analysis had to account for such factors as fiber properties, matrix properties, fiber volume fraction, and fiber ℓ/d ratio.

APPROACH

As described previously, this program was divided into experimental and analytical tasks. The experimental efforts included material fabrication and testing and the analytical efforts included failure theory evaluations and data correlations. The specific procedures that were employed in each task are outlined in the following paragraphs.

EXPERIMENTAL PROCEDURE

The experimental tasks were undertaken to determine qualitatively and quantitatively the failure behavior of a ceramic matrix composite. The experiments were planned to provide data that could be compared to several different failure theories. The testing program was designed to get as much data as possible from a limited amount of material.

The composites tested in this program consisted of an Al_2O_3 matrix reinforced with SiC whiskers. This combination of materials was chosen because the composites could be fabricated with relatively little difficulty. Furthermore, both constituents have been utilized in structural applications either as composite or monolithic materials. Therefore, the composites not only served as model materials but also possessed attractive mechanical material properties. The properties of the constituents are shown in table 1. The SiC whiskers used are manufactured by ARCO Metals-Silag Division and are designated as grade F-9. The whisker data shown in table 1a were obtained from reference 4 and are believed to be representative of the whiskers in the composites. Table 1b presents a range of properties of six commercial Al_2O_3's as reported in reference 5. The stiffness and fracture toughness of the matrix is very sensitive to void content, porosity, and grain size, reference 6. In general, as the void content and grain size decrease, the stiffness and fracture

toughness of the Al_2O_3 matrix increase. Therefore, in order to model the matrix material, it was necessary to determine the in-situ grain size from scanning electron microscope images and then choose the appropriate material properties. The composites were fabricated by Arco-Silag from a blend of Al_2O_3 powder and SiC whiskers. The aluminum powder was a standard Linde A with a particle size of less than 3 μm. As described previously, the SiC whiskers were Arco-Silag grade F-9. The constituents were combined to produce the correct volume fraction composites and blended until the mixture was homogeneous. The blends were then sent to Eagle-Picher Industries, Specialty Materials Division, Quapau, Oklahoma where they were hot pressed. The billets were pressed in parallel at 4000 psi. They were elevated to a temperature above 1750°C for a total of 90 minutes and held at a maximum temperature of 1860°C for 15 minutes. Unfortunately, the first two attempts to fabricate materials resulted in broken graphite dies which destroyed the materials. The third hot pressing was successful resulting in the three billets shown in figure 1. Each billet was cylindrical with a diameter of roughly 3.00 inches and a height of 1.50 inches. The rough edges shown in the photograph are due to irregularities caused by grafoil liners in the dies.

The materials were tested mechanically as single edge notched beams (SENB) loaded in four point bending. The materials were tested in bending to eliminate potential failures at the grips that occur in tensile tests of brittle materials. Four point bending was chosen to insure that the crack was in a pure bending stress field with zero shear stress. The specimen design followed the guidelines outlined in reference 7. The specimen, as shown in figure 2, was 1.75 inches long, 0.250 inches wide and 0.125 inches deep. The notch was located at the center of the tensile face and three initial crack depths were tested ($\frac{a}{W}$ = 0.25, 0.35 and 0.50). The load points were centered along the length and

separated by a distance of 0.875 inches resulting in what is typically referred to as a ½ four point bend test. That is, the distance between the support and load and the distance between the load and the beam midlength both equal ¼ of the beam length.

The test matrix included both notched and unnotched specimens as shown in table 2. Three different materials were tested as outlined in the test matrix. These included: an unreinforced matrix (Al_2O_3); a 10 v/o composite (10 SiC/Al_2O_3); and a 20 v/o composite (20 SiC/Al_2O_3). Beams were tested as machined and also with three different initial notch lengths. In general 5 specimens were tested for each material and each notch length. The unnotched, unreinforced material was tested using 10 specimens to determine statistically meaningful Weibull strength parameters. Each specimen was given a designation corresponding to its material, notch length and replication number as shown in table 2. For example, specimen A1 refers to replication number 1 of specimen design A. Specimen design A is the unreinforced material with no notch. This test plan resulted in a total of 65 mechanical tests.

The billets were machined into specimens by BOMAS Machine Specialties, Inc., Somerville, Massachusetts. Each specimen was cut to size and surface finished by grinding parallel to the long dimension with a 320 grit diamond final grind. The specimens were also notched at BOMAS by machining the notched simultaneously in all specimens. This was done to eliminate possible errors in measurement and to insure accurate data reduction.

The mechnical tests were performed at the Rutgers University Department of Ceramics. The bend tests were performed on an Instrom model TTCL-174 testing machine with a constant crosshead speed of 0.002 in/min. All tests were performed at room temperature. The data was collected in the form of measured load versus machine crosshead deflection. This method of deflection

measurement is not considered optimum. The potential inaccuracies will be discussed in a following section. However, the calculations of flexure strength and fracture toughness utilized only the maximum load and should not be affected by any deflection inaccuracies.

As shown in the test matrix, table 2, scanning electron microscopy (SEM) studies were performed on the materials. These were performed to qualitatively assess the failure modes in the composites and to examine the microstructure. The test matrix shows that 8 specimens were examined for each composite. These represented 2 specimens from each of the different notch length designs. The 2 specimens were chosen as the highest and lowest strength specimens from each material and notch configuration to investigate the possibility of different failure modes associated with different strength levels. The SEM specimens were prepared by mounting stubs using silver (Ag) paint followed by a sputter coating of gold (Au) to enhance the specimen conductivity. The specimens were examined to determine grain size fracture path, fiber dimensions, fiber spacing and constituent bonding.

The majority of the experimental data was employed to compute either flexural strength (i.e. modulus of rupture) or critical stress intensity. For the specimen shown in figure 2, the bending moment along the central span of the beam is given by:

$$M = \frac{P\ell}{8}$$

where,

P = total load recorded by test machine

ℓ = specimen length, 1.75 inches

Knowing the moment, the stress at failure for this specimen is;

$$\sigma_b^{ult} = \frac{3P_{max}\ell}{4BW^2}$$

where,

P_{max} = maximum load

W = Beam thickness, 0.125 inches

B = Beam width, 0.250 inches

The critical stress intensity factor, K_{IC}, was computed from an expression given in reference 8 which is applicable to SENB specimens in four point bending. The stress intensity factor is given by:

$$K_{IC} = \frac{3P_{max}\ell\sqrt{a}}{4BW^2}\left[1.992-2.468\left(\frac{a}{W}\right)+12.97\left(\frac{a}{W}\right)^2-23.17\left(\frac{a}{W}\right)^3+24.80\left(\frac{a}{W}\right)^4\right]$$

where,

a - crack length at which crack becomes unstable

These expressions were utilized to reduce the data that resulted from the mechanical tests. Bending strengths were determined from the unnotched specimens and fracture toughnesses were determined from the notched specimens.

ANALYTICAL HYPOTHESES

Several different theories were investigated to describe the failure behavior of the experimental materials. The theories included both explanations of fracture toughness and flexural strength. Since the materials are brittle, the strength theories are typically based upon principles of fracture mechanics. Thus,

the theories for fracture toughness and strength tend to have similar elements and there is no clear distinction between one and another. However, for the purposes of description, the failure theories that were investigated have been divided into five different categories. These theories have been referred to as: Tortuous Path; Strength vs. Size; Critical Matrix Stress; Crack Tip Damage Zone; and Inherent Crack Length. The following sections outline each of these theories and explain how they were compared to the experimental data.

Tortuous Path

The tortuous path theory attempts to explain the increase in fracture toughness that is typically seen in composite materials. This theory assumes that the crack grows through the matrix material but is diverted when it intersects the reinforcing whiskers. This concept is shown schematically in figure 3. The figure compares projected differences in behavior between a monolithic ceramic and a whisker reinforced ceramic. In the monolithic material the crack can grow perpendicular to the loading direction in a relatively straight line. This behavior is plotted in the accompanying crack growth resistance curve. The figure shows that for a given crack size the load can be increased with no crack extension until the critical stress intensity is reached. At the stress level corresponding to the critical stress intensity, the crack grows in an unstable manner and the specimen fails catastrophically.

On the other hand, the composite material is postulated to show a very irregular crack pattern as the crack grows around the reinforcing whiskers. The specimen is expected to exhibit a tortuous crack path as shown in the figure. As the crack changes direction its orientation to the applied stress will change and it will therefore require more energy (i.e. a higher stress) to propagate. This will result in a different crack growth resistance

curve as shown in the figure. In this case, the crack will begin to extend when the stress intensity reaches a given level. However, the crack will only extend at that stress until it intersects a whisker. Then it will change direction and stop since it will require more energy to propagate in the new direction. If the stress level is increased the crack will grow further until it intersects another whisker and the process will repeat. This will continue until a point at which the applied stress intensity is large enough to fail both the matrix and the whiskers and then the crack will grow catastrophically.

If the tortuous path approach is realistic, the experimental data should show certain trends. It is expected that the monolithic ceramic will exhibit a linear, brittle load-deflection curve. The composite is expected to show some nonlinearity which would be evidence of stable crack growth. The composite crack path should appear to be jagged and irregular, the SEM photographs should show unbroken whiskers, and crack growth should occur predominately through the matrix.

This theory can be evaluated numerically by assuming an idealized crack path. For example, the path may be taken as a sine wave where the amplitude and period of the path are related to the microstructure of the composite. The total energy required for the crack to traverse this path can be taken as the integral along the sine wave accounting for variations in the energy due to crack direction changes. This total energy can then be related to an effective critical stress intensity which should be equivalent to the measured composite stress intensity.

Strength vs. Size

The strength vs. size theory attempts to explain the increase in strength that is expected as the volume fraction of reinforcement is increased. This hypothesis assumes that composite failure

is caused by failure of the matrix material. Since the matrix is a brittle material, its strength can be described in statistical terms related to the size of the specimen. In other words, it is assumed that the strength of a brittle material is limited by the presence of defects, reference 9. As the size of the specimen increases, the probability that the specimen contains a critical defect increases. This implies that the measured strength of a brittle material should decrease as the size of the specimen increases, figure 4.

In order to apply this to the ceramic composites, it was necessary to determine the Weibull curve fit parameters for the unreinforced matrix material. Then it was assumed that the whiskers acted to transfer stress through the matrix material. This in effect decreases the size of the specimen. For the purposes of applying this theory, the size of the matrix material was taken as the average unreinforced volume of matrix within the composite. This volume dimension is a function of the reinforcement volume fraction and size. Once the average matrix volume was calculated it could be applied to the matrix strength distribution to predict the composite strength. If this hypothesis was valid, the calculated strengths should match the measured strengths and the SEM photographs should show predominately matrix failure.

Critical Matrix Stress

The critical matrix stress theory focuses upon the strength of ceramic matrix composites, but may also explain increases in composite fracture toughness. This theory treats composite failure as a combination of matrix and whisker failure. It is assumed that at a given stress state, small cracks appear in the matrix. These cracks are prevented from growing catastrophically by the presence of the whiskers. As shown in figure 5, the accumulation of cracks within the matrix reduces the matrix stiffness. This

transfers load from the matrix to the stronger whiskers, and should appear as a nonlinear composite load-deflection curve. As the applied stress is increased, the matrix accumulates more damage, reducing its stiffness and transferring more load to the whiskers. This process continues until a critical matrix stress is reached when the existing damage propagates catastrophically causing final failure.

This hypothesis can be tested experimentally by measuring the load-deflection response of two composites with different whisker volume fractions, figure 5. If damage accumulation in the matrix is a viable hypothesis, the composites should exhibit some nonlinear behavior. If the composite stress-strain curve is used to compute the effective matrix stress-strain curve, both composites should result in the same effective matrix response. In other words, if the instantaneous stiffnesses of the constituents are known, it should be possible to compute the composite behavior by volume averaging. Thus, the difference in the measured behavior for the two composites should be related directly to the difference in whisker volume fraction.

This theory can be simplified by assuming that both constituents behave linearly to failure. In this case, the composite will fail when the average stress in either constituent reaches the corresponding ultimate strength. For example, the composite may fail when the average matrix stress reaches the allowable matrix strength. This concept can be tested by estimating constituent allowables from the tests on one composite and using them to predict the behavior of the other composite. This, of course, is only applicable if the composite exhibits a linear stress-strain curve.

Crack Tip Damage Zone

The crack tip damage zone theory is based upon a composite fracture concept proposed by Waddoups, reference 10. It is assumed

that a region of damaged material exists at the tip of the crack. Because of the damage this material is very compliant and transfers very little stress. This, in effect, increases the length of the crack and this increase must be accounted for when determining the fracture toughness of the material or when using fracture mechanics to design structures. The damage zone is expected to be related to the microstructure of the composite and should decrease in size as the volume fraction of whiskers increases. It is expected that one value of critical stress intensity, K_{IC}, could be determined for all similar composites and the difference in measured K_{IC} could be accommodated by varying the damage zone size.

This theory can be easily tested by examining the fracture data for the two composite systems. The data is plotted in the form of fracture stress versus crack size. It is assumed that the actual crack size is actually $a+a_o$, where a is the measured crack and a_o is the dimension of the damage zone. The data is fit to curves of stress versus crack size by varying the parameters K_{IC} and a_o. Then the curve fit parameters for the two composite systems are compared. As described, it is expected that K_{IC} should be nearly the same for the two composites, a_o should be a dimension on the order of the microstructure and a_o should decrease as the volume fraction increases.

Inherent Crack Length

The inherent crack length theory, reference 11, assumed that failure of a composite containing brittle constituents is caused by catastrophic growth of existing flaws. The theory treats composite failure as failure of the matrix and assumes that the whiskers limit the size of the inherent flaw. This material model assumes that the length of the inherent flaw is equivalent to the mean free path between the whiskers. For elliptical whiskers,

the mean free path is approximately:

$$\ell = \frac{4}{3} a \left(\frac{b}{a}\right)^{\frac{2}{3}} \left(\frac{1}{V_r} - 1\right)$$

where,

a - whisker diameter

$\frac{b}{a}$ - whisker aspect ratio

V_r - whisker volume fraction

The critical stress intensity of the matrix is then employed in a fracture mechanic expression to predict the composite strength.

$$\sigma = \frac{K_{IC}}{f\left(\frac{\ell}{w}\right)\sqrt{\pi \ell}}$$

where,

K_{IC} - matrix critical stress intensity

ℓ - mean free path

$f\left(\frac{\ell}{w}\right)$ - function of the crack geometry

This theory is easily tested by predicting composite strengths as a function of whisker volume fraction and aspect ratio. The predicted strength can be compared to the measured flexure strength to evaluate the model.

RESULTS

The technical results generated during this program consist of experimental data and evaluation of analytical predictions. The following sections outline the measured mechanical data and theoretical calculations.

EXPERIMENTAL DATA

The experimental results consisted of load-deflection curves from flexure tests and SEM micrographs of the failure surfaces. The detailed data is contained in an Appendix to this report. This section describes the highlights of the experimental study including typical SEM features, typical load-deflection curves and average measured properties.

The materials were fabricated as outlined in the approach section. Before the specimens were machined, the density of each billet was measured and compared to the theoretical density for the composite. These results are presented in table 3. The tabulated values show that all materials densified well. Only the 20% composite showed any significant density loss (98% theoretical density) and this is probably due to the whiskers which prevent complete compaction of the matrix. This may lead to slightly lower strengths and fracture toughnesses than could be obtained with a fully dense composite. The processing parameters appear to have produced good quality composites.

Failure surfaces typical of the composites are shown in figures 6 through 8. Figure 6 presents views of the unreinforced Al_2O_3, figure 7 presents views of the 10% SiC/Al_2O_3, and figure 8 presents views of the 20% SiC/Al_2O_3. These figures were all taken from the unnotched specimens ($\frac{a}{w}$ =0.0). The notch length had no noticeable effect on the SEM micrographs of the failure surfaces so these figures can be treated as typical of the mater-

ial microstructure.

The SEM study uncovered several interesting aspects of the materials. Notice that the magnification of the unreinforced micrographs, figure 6, range from 50X to 1000X while the composites, figures 7 and 8, were taken under magnifications of 2500X to 10,000X. The grain sizes in the unreinforced Al_2O_3 are very large, on the order of 1mm, and there appears to be significant intergranular cracking. The grain sizes in the composite SEM's, figures 7 and 8, are much smaller. Thus, it appears that the whiskers acted as grain growth inhibitors. The large grain size in the Al_2O_3 is probably due to processing parameters. The difference in microstructure implies that the properties determined from the unreinforced Al_2O_3 are not representative of the Al_2O_3 that is found in the composites.

The SEM micrographs of the composites, figures 7 and 8, show clear views of the SiC whiskers and surrounding matrix. Clearly, more whiskers are evident in the 20% composite than in the 10% composite. The whiskers are seen to be sticking out of the surrounding matrix as if they pulled out of the opposite fracture surface. Further evidence of whisker pull-out is seen in the holes and indentations on the fracture surface. Except for the increase in whisker content there are no major differences in the fracture surface between the 10% and 20% materials. Failure seems to have occurred within the matrix. The whisker-matrix bond appears to be solid and, except for the agglomerated whiskers in figure 8, there is little evidence of voids or porosity. Based upon these micrographs, it may be concluded that the failure occurred by crack growth through the matrix. The whiskers appear to have pulled out on final fracture. There is very little evidence of whisker fracture.

The load-deflection behavior of the flexure specimens is outlined in figures 9 through 13. Figure 9 represents the data from a typical unnotched, unreinforced specimen. Figure 10 is a corresponding plot for a notched unreinforced specimen. These figures

are typical of the measured data. Tabulated data for each specimen are detailed in the appendix. In general, the load-deflections of the unreinforced Al_2O_3 showed an initial linear region followed by some decreased stiffness as the specimens reached the maximum load. The secondary loading that appears in figure 9, although typical of the other unnotched, unreinforced specimens, is believed to be an artifact of the testing procedure and is not representative of material behavior. The maximum load reached by both the unnotched and notched Al_2O_3 is much lower than expected. Similarly the initial slope (stiffness) is very low. It is believed that the microcracks seen in figure 6 act to reduce the effective stiffness and strength of the material and this is the cause for the low slopes and loads.

The corresponding composite load-deflection curves are shown in figures 11, 12, and 13. Figure 11 is typical of unnotched composites, figure 12 is typical of low notch depths (a/w=0.25, 0.35) and figure 13 is representative of the largest notch (a/w= 0.50). Again, these figures are typical of the data. Detailed information is supplied in the appendix. The composites with no notch or small notches, figures 11 and 12, are characterized by an initial linear slope, followed by a zero stiffness plateau that occurs at a load of 20-25 lbs, followed by another linear loading to failure. The large notch specimens, figure 13, are characterized by a linear load to failure.

The plateau is believed to be due to slippage in the test fixture or an error in the measurement of crosshead deflection. Another potential cause, bearing failure under the load points, was ruled out when no evidence of crushing was found on the failed specimens. If the plateau was caused by material failure, the secondary slope should be significantly lower than the initial slope. Also, the fact that the plateau occurs at the same load for both 10% and 20% composites, points towards a fixture response as opposed to a material response. This is supported by the specimens

with deep notches which failed at a load lower than the plateau load. Thus, for the purposes of material evaluation, it is believed that the composites were linear, elastic, brittle materials.

The load-deflection curves show no evidence of nonlinearity immediately prior to failure and the drastic drop in load implies catastrophic brittle fracture. Although, the unreinforced Al_2O_3 showed very low stiffness and strength, the composite values appear to be more reasonable in terms of the constituent properties, table 1.

The load-deflection curves were utilized to measure stiffnesses, maximum loads and deflections at maximum load. These measurements are summarized in table 4. In examining the maximum load, notice that the load to failure decreases as the notch depth increases, as expected. Also notice that the failure load increased as more whiskers are added to the composites implying that the whiskers do act to strengthen and toughen the composites. As mentioned previously, the unreinforced Al_2O_3 exhibit very low failure loads (as low as 10% of the corresponding composite failure load) because of microcracking. The stiffnesses and maximum deflections are based upon crosshead deflections so the accuracy is questionable. When the stiffness is calculated for the composites based upon simple rule-of-mixtures models, it is found that the difference between the two composite moduli is about 5%. Thus, even though the 20% composite is expected to be stiffer than the 10% composite, the theoretical difference is so small that it may be lost in the scatter of the data.

As described in the approach, the maximum load was utilized to calculate flexural strength and critical stress intensity for the materials. The average values of these calculations are shown in table 5. The flexural strength shows the expected increase with whisker content. Similarly, the critical stress intensity increases with whisker content. The low strength and K_{IC} for the Al_2O_3 are caused by the microcracking and are not representative of commercial Al_2O_3 or in-situ matrix. The composite K_{IC} values

of 3.0 to 4.0 ksi $\sqrt{in}$ appear to be reasonable when compared to the constituent K_{IC}'s, table 1. Also, as shown on figure 14, the computed K_{IC} values were dependent on whisker content yet relatively constant with crack size.

In summary, the experimental data have led to several conclusions. The fabricated materials exhibited reasonable densities which imply that the composites were well manufactured and good quality materials. The SEM micrographs show that failure occurs predominately through the matrix with little or no evidence of whisker fracture. The load-deflection data leads to the conclusion that the composites are linear, elastic, brittle materials. The failure data shows that the flexural strength and critical stress intensity is increased as the reinforcement content is increased.

ANALYTICAL COMPARISONS

The experimental data were compared to the material behavior projected by the theories discussed in the approach section. The theories were designated as: Tortuous Path; Strength vs. Size; Critical Matrix Stress; Crack Tip Damage Zone; and Inherent Crack Length. The following paragraphs outline the results of those comparisons.

The tortuous path hypothesis projected stable crack growth and nonlinear load-deflection behavior for the composites. Since the materials failed catastrophically with no evidence of nonlinearity, this theory does not appear to be valid. Although the cracks appear to grow around the whiskers, the change in energy associated with this change in direction was apparently insufficient to cause stable crack growth.

The strength versus size theory is based upon knowledge of the in-situ matrix Weibull parameters. Unfortunately, the unreinforced Al_2O_3 possesses a grain size which is much larger than the in-situ matrix. Therefore, the Weibull parameters obtained for the Al_2O_3 material can not be applied directly to the matrix.

Although the model qualitatively describes the observed behavior in that it projects brittle failure and increasing strength with volume fraction, it can not be tested quantitatively without knowledge of the matrix Weibull parameters.

Comparisons between the critical matrix stress theory and the experimental data are shown in figures 15 through 17. The theory assumes that the composite fails when the average matrix stress reaches a limiting value. The three figures outline the procedure that was used to determine the matrix behavior from the 10% composite and use that information to predict the composite behavior for the 20% material. Figure 15 presents stress-strain curves for 10% SiC/Al_2O_3 derived from load-deflection curves on unnotched beams. The figure shows an average 10% composite stress-strain response that was determined from data measured on several beams.

The average 10% composite behavior was employed to determine the average matrix stress-strain response as shown in figure 16. The whisker stress-strain response was determined from the reported whisker modulus table 1, and projections of whisker strength. From figure 16 it can be seen that the composite failed at a stress of about 38 ksi and a strain of about 750$\mu\varepsilon$. Assuming that this failure represents matrix failure and using simple rule of mixtures this implies that the matrix fails at an average stress of about 36 ksi.

The matrix response was then utilized to predict the behavior of the 20% composite. The comparison of the predicted to measured response is shown in figure 17. The predicted 20% composite fails at a stress of about 40 ksi. The measured 20% composite however, has an average strength of 50 ksi. This paradox can not be explained by the critical matrix stress theory. Although, the constituents appear to carry stresses proportional to their moduli as evidenced by the agreement between predicted and measured stiffness, the composite strengths can not be computed

from a simple matrix stress criterion.

The crack tip damage zone postulates that fracture of the composites can be predicted by considering a micromechanical damage zone at the crack front which reduces the fracture load of the materials. This hypothesis implies that the composites may have similar K_{IC} values, yet different damage zone sizes. It is expected that the damage zone lengths should be related to the size of the composite microstructure. Furthermore, it is expected that the damage zone length should decrease as the whisker content increases. This theory was tested by allowing the crack length to be equal to $a+a_o$, where a_o is the damage zone length. Using this hypothesis the composite fracture stress versus crack length data were fit to empirical relationships to determine K_{IC} and a_o.

The results are shown in figures 18 and 19. Figure 18 shows that data and curve fit parameters for the 10% composite and figure 19 shows similar results for the 20% composites. The curve fits require a K_{IC} of 6.03 ksi $\sqrt{in}$ for the 10 SiC/Al_2O_3 material and a K_{IC} of 8.92 ksi $\sqrt{in}$ for the 20 SiC/Al_2O_3 material. The computed damage zone size increases from 0.0275 inches for the 10% composite to 0.0325 inches for the 20% composite. Clearly the computed damage zone sizes are very large when compared to a composite with a microstructure on the order of microns. Also, the damage zone size does not decrease with increasing whisker content and the computed K_{IC} values are significantly different. Therefore, the damage zone concept does not appear to be useful in assessing failure of the composites.

The inherent crack length theory assumes that failure of the composites is caused by fracture initiated at some inherent flaw. The theory also assumes that the flaw size is equal to the mean free path between the whiskers in the composite. For the composites measured here, the mean free path was computed as outlined in the approach. The strength of the composites was then predicted by employing this flaw size in a linear elastic fracture

mechanics calculation. The computed flexural strengths are compared to measured data in figure 20. The curve shows computed strength versus whisker volume fraction with whisker aspect ratio as a parameter. The calculations are based upon an average whisker diameter of 0.6μm and a matrix critical stress intensity of 3.50 $\sqrt{in}$. These values were taken as average constituent properties and are consistent with the data presented in table 1. The calculations show good agreement for whiskers with an average aspect ratio of 30. This correlates with the average value reported in table 1. Therefore, the inherent crack length theory appears to have validity for predicting the strength of these composites.

This model of the ceramic composite failure behavior has several implications. First, as shown in figure 20, the strength of the materials will increase as the volume fraction increases. A more interesting trend is that the strength increases as the reinforcement aspect ratio decreases. This is because, at the same volume fraction, the mean free path between low aspect ratio particles is smaller than the mean free path between large aspect ratio particles. Thus, the model implies that particle reinforced ceramics should be stronger than whisker reinforced ceramics.

The limitation to this model is that it does not account for any strength contribution from the whiskers. For these particular composites that appears reasonable, since the whiskers appear unbroken in the SEM's. However, if the whisker length is increased, the tendency for the whiskers to pull out will be diminished. At some point the composite strength will begin to reflect failure of the whiskers and this model will no longer be valid. However, for whiskers and particles which are presently fabricated, the model has potential as a strength assessment tool.

In summary, the comparisons of several theories to the experimental data showed that the present best explanation of the failure behavior of ceramic composites is the inherent flaw model. The model predictions agree well with data on SiC/Al_2O_3 composites.

The trends predicted by the model imply that composite strength can be improved by increasing the whisker volume fraction or making the reinforcement material more spherical in shape. The theories based upon subcritical micromechanical damage such as the damage zone and tortuous path do not appear to accurately model the material response. Also, failure theories based upon an average constituent stress appear inadequate.

CONCLUSIONS AND RECOMMENDATIONS

The results of this study have led to several conclusions regarding the failure/fracture behavior of whisker reinforced ceramic composites.

The experimental study showed that it is possible to fabricate SiC/Al_2O_3 ceramic composites with reasonable final densities and good microstructure. The mechanical data showed that the materials are linear to failure, exhibiting no nonlinearity or stable crack growth. The measured strength and fracture toughness of the composites increased with increasing volume fraction. The unreinforced Al_2O_3 materials exhibited very low stiffness, strength and fracture toughness. This was believed to be caused by the very large grain size and microcracking seen in the Al_2O_3 SEM micrographs. The SEM micrographs of the SiC/Al_2O_3 composite showed a much smaller matrix grain size as if the whiskers acted as grain growth inhibitors. The fracture surfaces show evidence of matrix failure and whisker pull-out which implies that failure of the material is matrix dominated.

The analytical theory which best explains the measured strength of the composites is based upon fracture of inherent flaws which are the size of the mean free path between whiskers. The model, within limits, predicts that the composite strength will be increased as the whisker content is increased and the whisker aspect ratio is decreased. Models of fracture behavior, which are based upon micromechanical damage growth within the composites, do not correctly simulate the measured behavior.

In order to further investigate these materials several concepts can be investigated. To further test the validity of the inherent flaw model, particle reinforced composites should be fabricated and tested. The model is also presently limited in that it accounts for no whisker failure. While that appears to be sufficient for the whisker reinforced materials

tested here, it may be not accurate for longer whiskers or continuous fibers. Thus, the model should be improved and compared to available data on continuous fiber reinforced ceramics. In order to investigate improvements in material properties, it is suggested that investigations focus on high strength matrix, whisker-matrix bonding, and longer whiskers. The SEM micrographs show that the failure occurs almost entirely through the matrix. Therefore, the composite behavior can be improved by either strengthening the matrix or forcing the whiskers to fail.

REFERENCES

1. Gray, A., "Materials Substitution: Challenge of the 80's," Metal Progress, v. 117, no. 2, pp. 32-37, February 1980.
2. Freche, J.C., and Ault, G.M., "Progress in Advanced High Temperature Turbine Materials, Coatings, and Technology," NASA TM X-73628, 1977.
3. McGarry, F.J., Rowe, E.H., and Riew, C.K., "Improving the Crack Resistance of BMC and SMC," Proceedings of the 32nd Conference of the Society of Plastics Industries, Section 16-C, February 1977.
4. Arco Metals-Silag Division, Grade F-9 SiC Whiskers Product Data Bulletin, September 1982.
5. Barker, L.M. "Short Rod K_{IC} Measurements of Al_2O_3," Presented at International Symposium on Fracture Mechanics of Ceramics, Penn State University, July 1977.
6. Rice, R.W., Frieman, S.W., and Becher, P.F., "Grain-Size Dependence of Fracture Energy in Ceramics: I-Experiment," Journal of American Ceramic Society, v. 64, no. 6, pp. 345-350, June 1981.
7. Baratta, F.I., "Requirements for Flexure Testing of Brittle Materials," AMMRC TR 82-20, April 1982.
8. Brown, W.F., Jr, and Srawley, J.E., Plane Strain Crack Toughness Testing of High Strength Metallic Materials, ASTM STP 410, February 1967.
9. Weibull, W., Proceedings Royal Swedish Institute for Engineering Research, no. 151, 1939.
10. Waddoups, M.E., Eisenmann, J.R., and Kaminski, B.E., "Macroscopic Fracture Mechanics of Advanced Composite Materials," Journal of Composite Materials, v. 5, pp. 446-455, October 1971.
11. Broutman, L.J., and Krock, R.H., eds. Modern Composite Materials, Addison-Wesley, pp. 72-75, 1967.

Table 1. Material Properties of Constituents used in SiC/Al_2O_3 Ceramic Composites

1a Whiskers, reference 4

Material -	E Msi	ν -	ρ gm/cc	K_{IC} ksi$\sqrt{in}$	Diameter Range μm	Average Diameter μm	Aspect Ratio Range -	Average Aspect Ratio -
SiC (F-9)	63.5	0.17	3.21	3.46	0.3-1.3	0.6	8-130	30.0

1b Matrix, reference 5

Material -	Modulus Range Msi	ν -	Density Range gm/cc	Grain Size Range μm	K_{IC} Range ksi$\sqrt{in}$
6 Commercial Al_2O_3	32.1-57.0	0.3	3.4-3.99	2-50	2.71-4.01

Table 2. Experimental Tests used to study SiC/Al_2O_3 Ceramic Composites

Material -	SiC Content v/o	Flexure $\frac{a}{W} = 0.0$	Flexure $\frac{a}{W} = 0.25$	Flexure $\frac{a}{W} = 0.35$	Flexure $\frac{a}{W} = 0.50$	SEM -
Al_2O_3	0	Spec. A1-A10	D1-D5	G1-G5	J1-J5	8
10 SiC/Al_2O_3	10	Spec. B1-B5	E1-E5	I1-I5	L1-L5	8
20 SiC/Al_2O_3	20	Spec. C1-C5	F1-F5	H1-H5	K1-K5	8

Total of 65 mechanical tests

Table 3. Fabricated Material Densities of SiC/Al_2O_3 Ceramic Composites

Material -	SiC Content v/o	Measured Density gm/cc	Theoretical Density gm/cc	Percentage of Theoretical Density
Al_2O_3	0	3.97	3.97	100
10 SiC/Al_2O_3	10	3.88	3.894	99.6
20 SiC/Al_2O_3	20	3.74	3.818	98.0

Table 4. Summary of Experimental Data on SiC/Al_2O_3 Materials

Notch Depth a/W	Specimen -	SiC v/o	Stiffness, $^{*}10^{3}$ lb/in		Max. Load, lbs		Δ^{*} at Max. Load, 10^{-3}in	
			Avg.	Sdev.	Avg.	Sdev.	Avg.	Sdev.
0.0	A	0	6.87	1.02	10.3	1.34	2.19	0.69
	B	10	26.6	2.01	104	26.0	8.03	1.24
	C	20	24.7	2.88	150	22.6	9.96	0.42
0.25	D	0	5.82	0.93	8.10	0.72	1.81	0.32
	E	10	15.9	0.35	32.1	1.33	5.19	0.12
	F	20	15.5	0.41	42.6	2.02	5.84	0.22
0.35	G	0	5.55	1.15	5.02	0.71	1.33	0.09
	I	10	14.4	1.43	18.9	0.56	2.62	0.34
	H	20	11.9	0.35	24.0	1.26	5.35	0.22
0.50	J	0	4.47	0.79	2.93	0.40	1.16	0.19
	L	10	12.5	0.77	12.6	0.45	1.01	0.04
	K	20	12.1	0.84	15.8	0.50	1.35	0.18

*Crosshead Deflections

Table 5. Summary of Experimentally Measured Failure Behavior of SiC/Al_2O_3 Materials

Flexural Strength

Specimens	SiC	σ_b^u, Ksi	
-	v/o	Avg.	Sdev.
A	0	3.45	0.45
B	10	34.9	8.73
C	20	50.3	7.60

Fracture Toughness

Specimens	Sic	K_{Ic}, Ksi $\sqrt{in}$	
-	v/o	Avg.	Kdev.
D, G, J	0	0.77	0.15
E, I, L	10	3.09	0.44
F, H, K	20	3.97	0.67

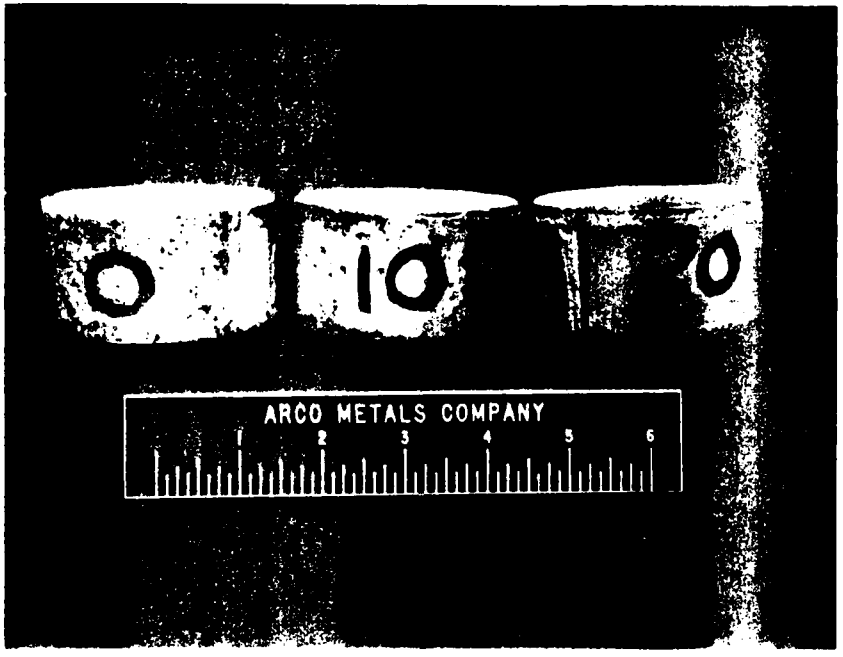

Figure 1. Macrophotograph of Ceramic Billets Containing 0%, 10%, and 20% SiC whiskers in Al_2O_3 Matrix.

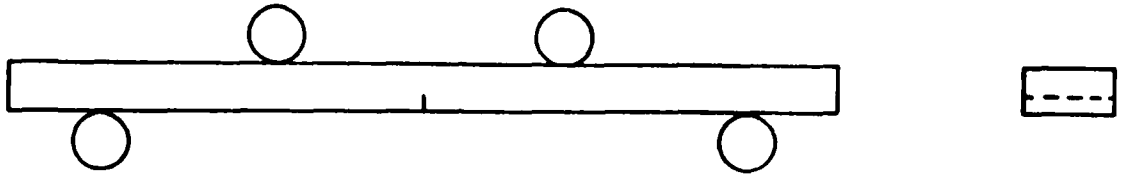

Scale 2:1

Total length	= 2.250"	Thickness	= 0.125"
Test length	= 1.750"	Width	= 0.250"
Loading length	= 0.875"	Roller radius	= 0.150"
Loading speed	= 0.002 in/min	Initial crack length	= 0.0, 0.031, 0.044, 0.063

Figure 2. Four Point Test Specimen

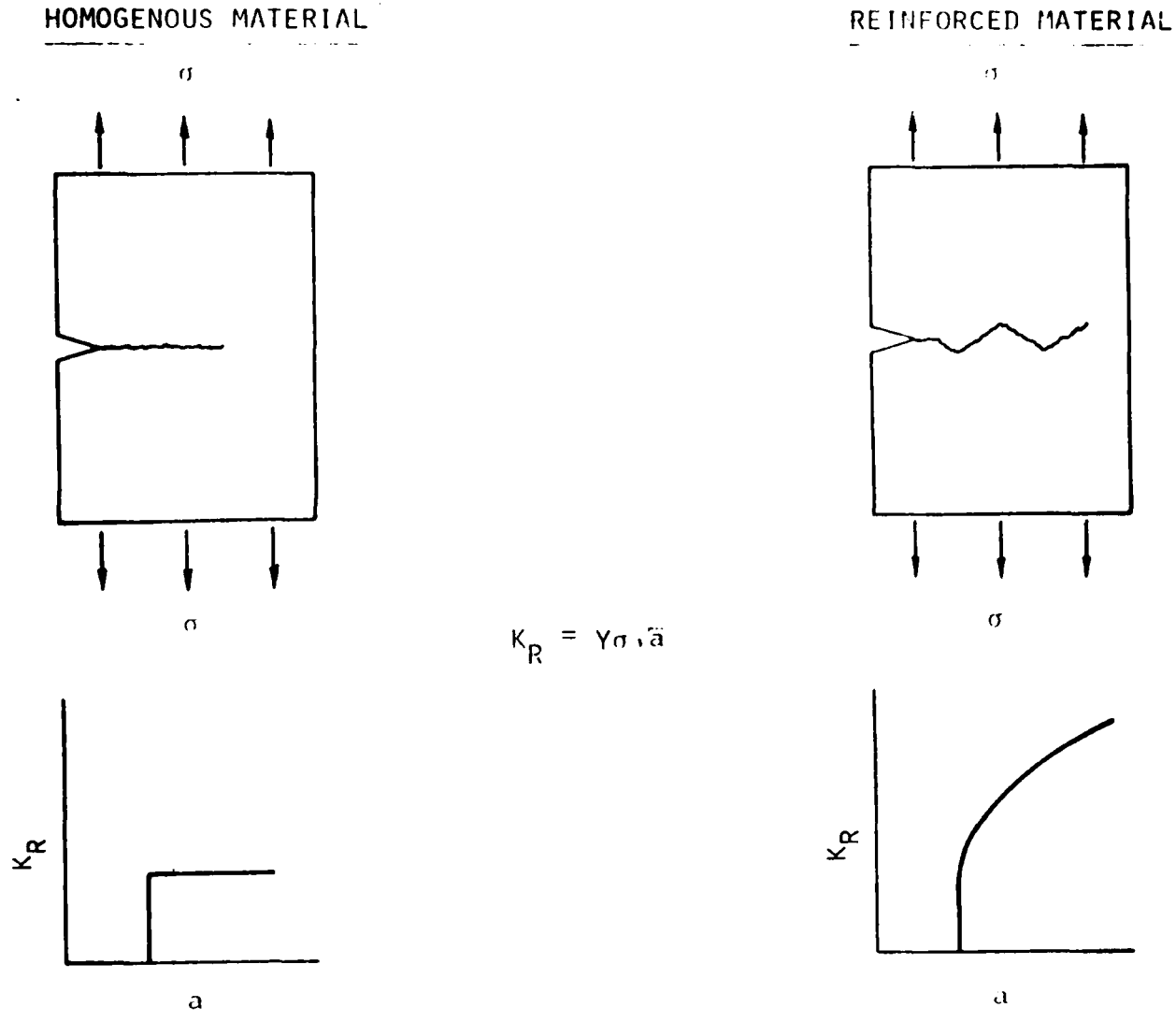

Figure 3. Schematic of Tortuous Path Hypothesis of Fracture in Ceramic Composites

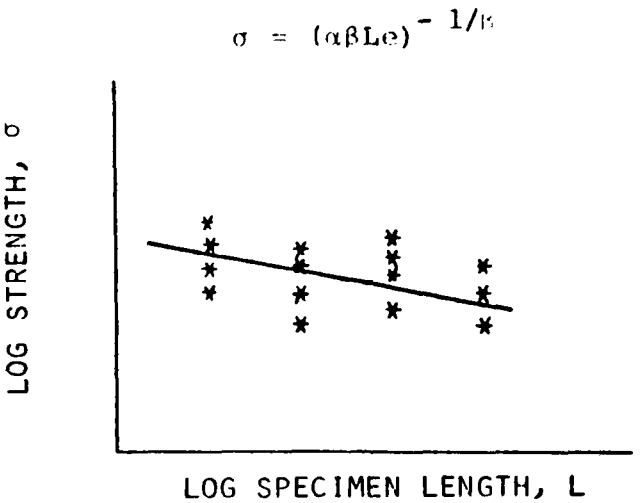

- DETERMINE WEIBULL PARAMETERS FROM HOMOGENOUS CERAMIC TESTS
- ESTIMATE PARTICLE SIZE FOR REINFORCED MATERIAL
- EXTRAPOLATE REINFORCED STRENGTH BASED UPON PARTICLE SIZE AND COMPARE TO EXPERIMENTS

Figure 4. Schematic of Strength vs. Size Hypothesis for Ceramic Composites

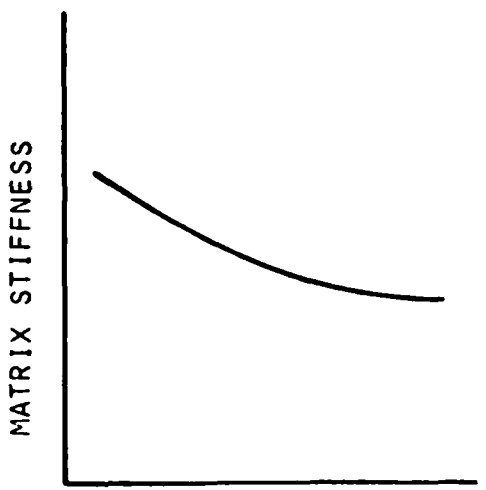

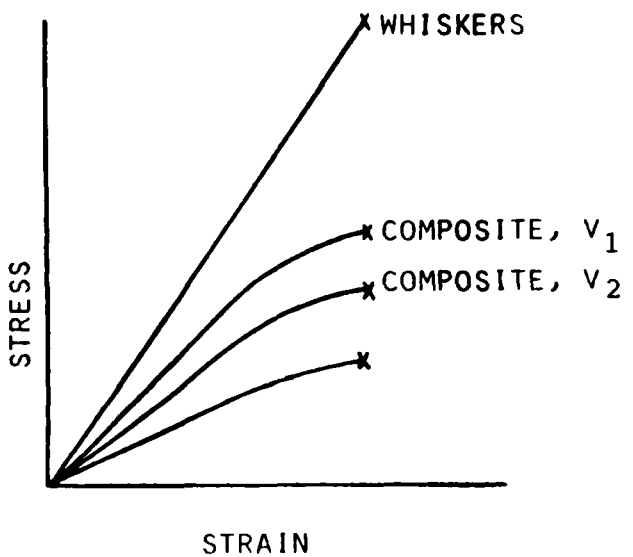

- MATRIX STIFFNESS WILL DECREASE AS CRACK DENSITY INCREASES

- WHISKERS WILL ACT AS CRACK ARRESTORS, REDUCING CRACK DENSITY

- RESULTING COMPOSITE WILL SHOW NON-LINEAR STRESS-STRAIN RESPONSE THAT IS A FUNCTION OF THE WHISKER VOLUME FRACTION

Figure 5. Schematic of Critical Matrix Stress Hypothesis for Ceramic Composites

50X

100X

1000X

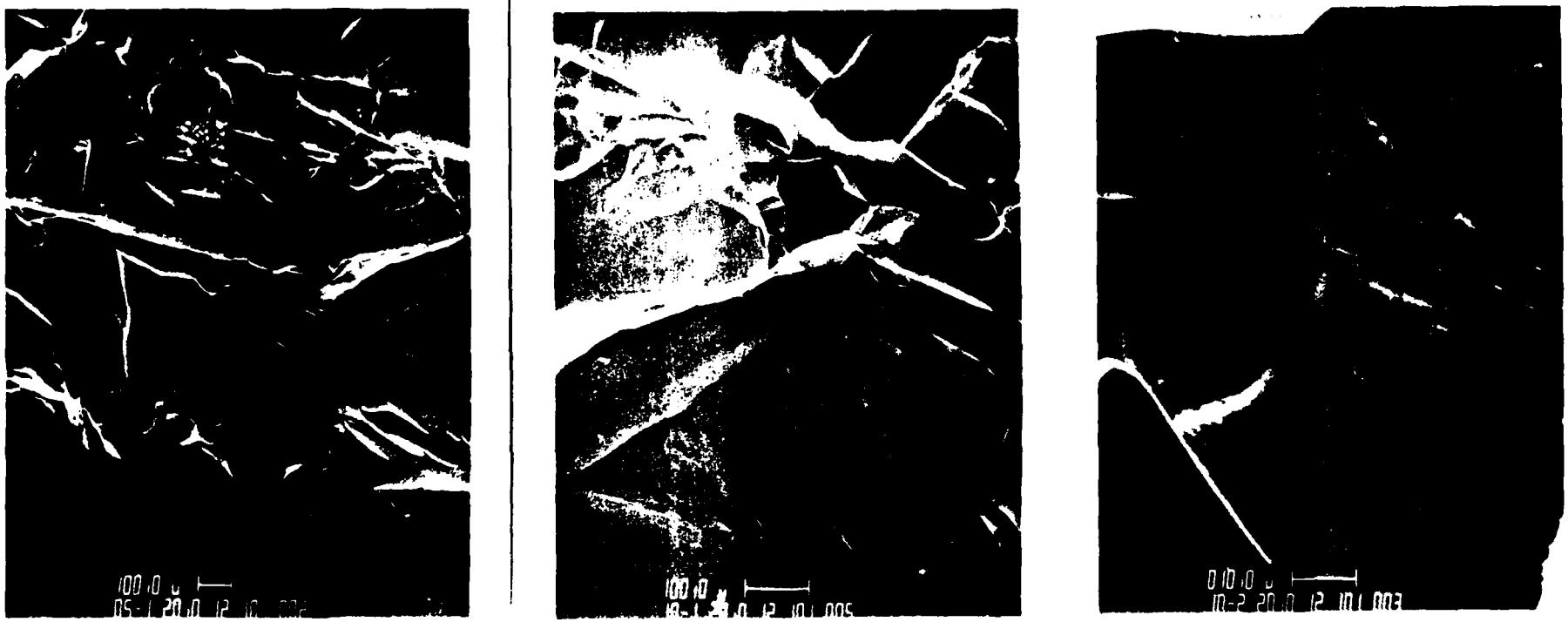

Figure 6. Fracture Surface of SiC/Al_2O_3 Composite
(0% SiC, a/W =0.0)

2500X

5000X

10,000X

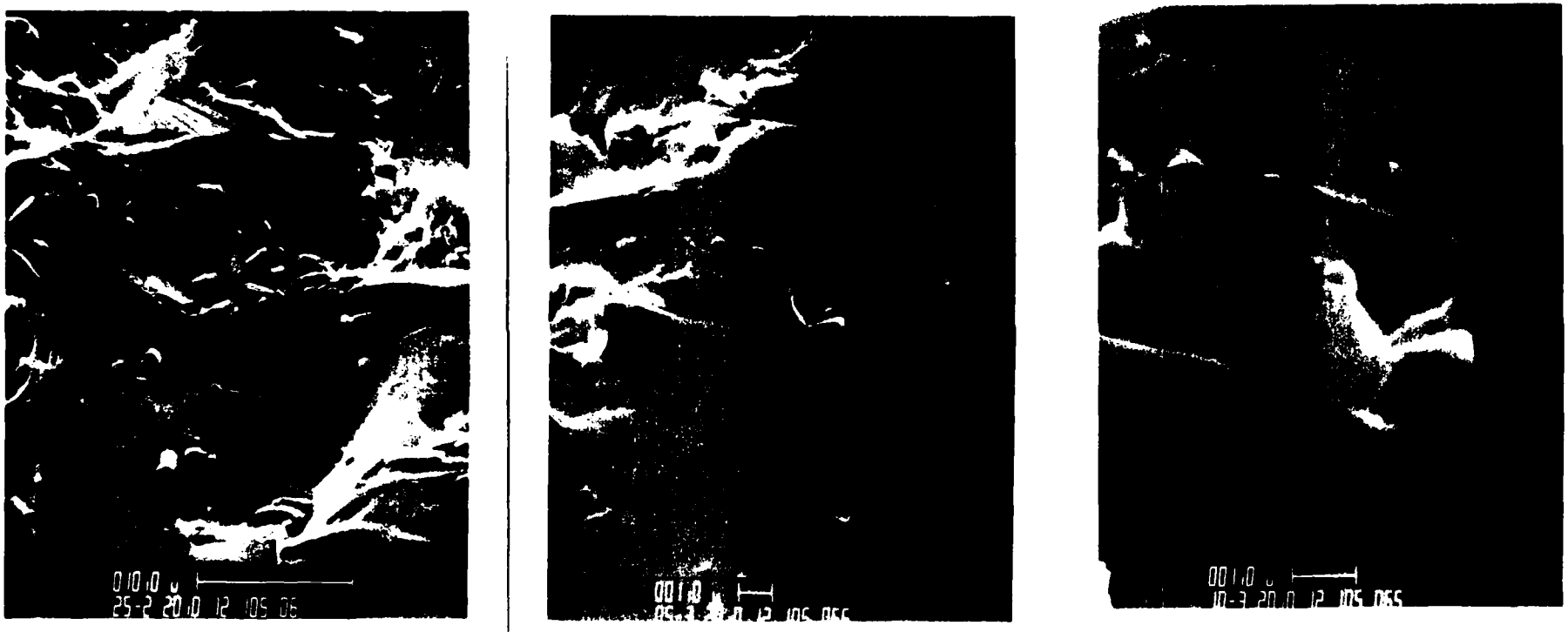

Figure 7. Fracture Surface of SiC/Al_2O_3 Composite (10% SiC, a/W =0.0)

2500X

5000X

10,000X

Figure 3. Fracture Surface of SiC/Al_2O_3 Composite (20% SiC, a/W =0.0)

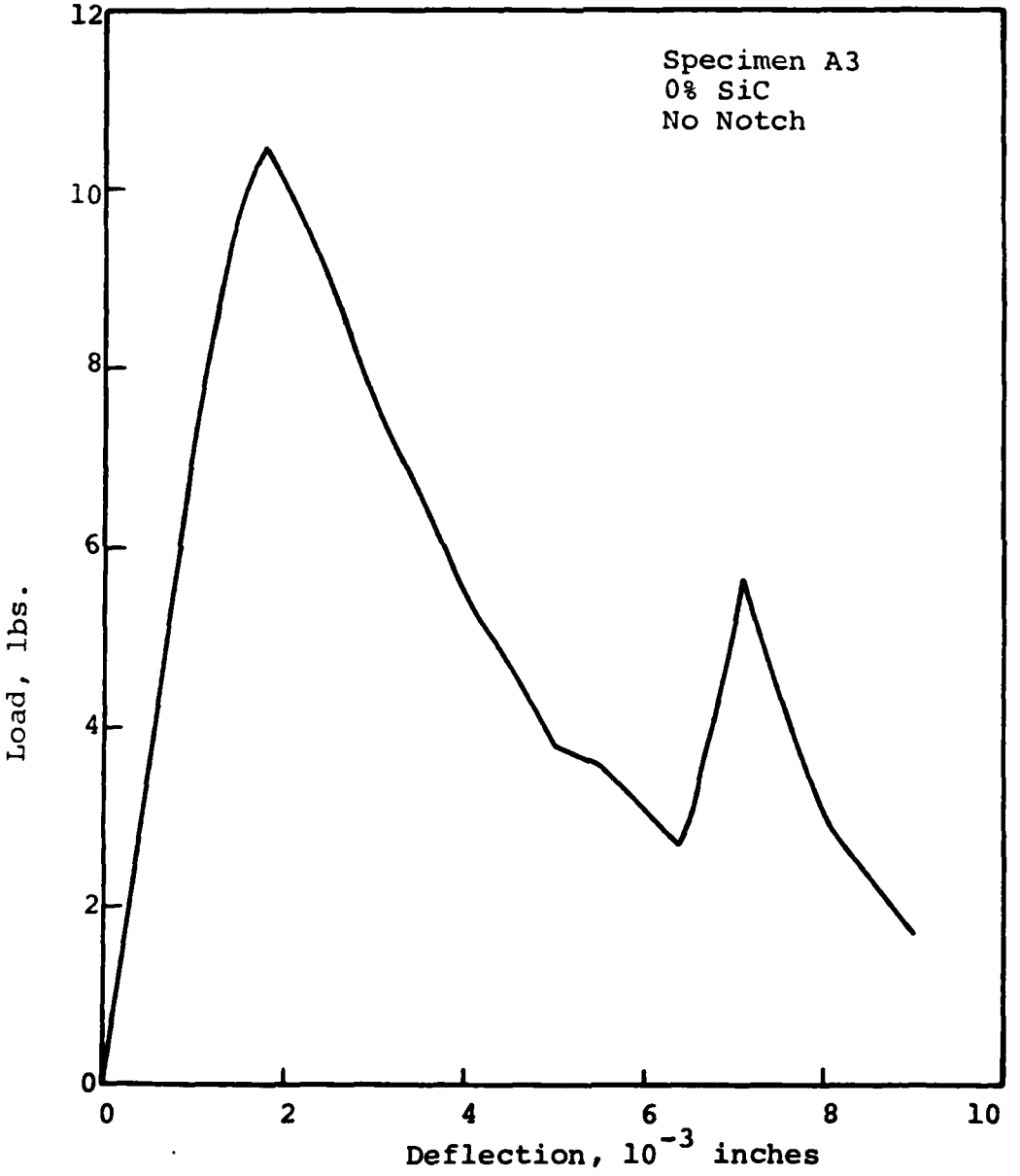

Figure 9. Load - Deflection response typical of unreinforced Al_2O_3 with no notch

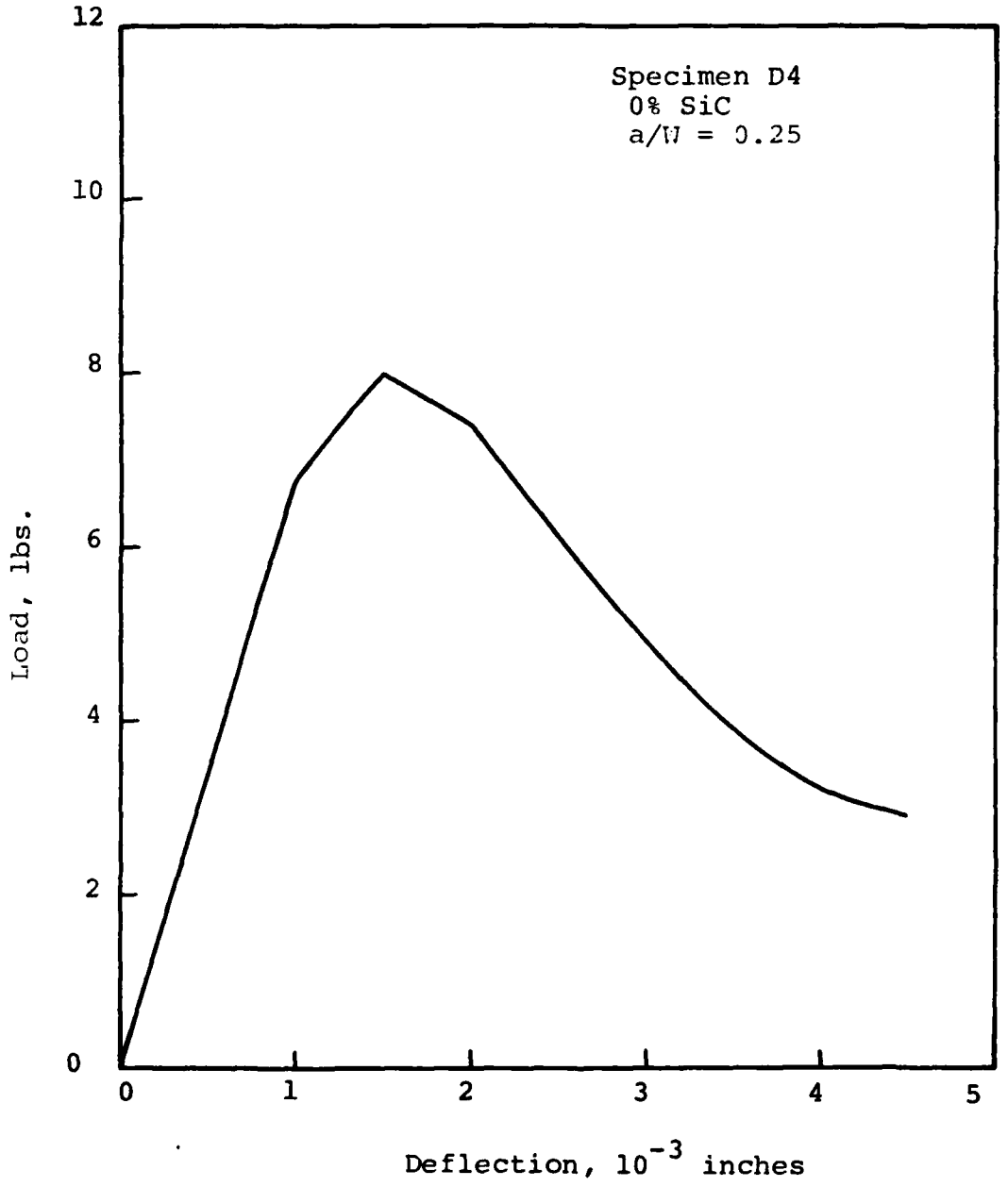

Figure 10. Load - Deflection response typical of unreinforced Al_2O_3 with notched specimens

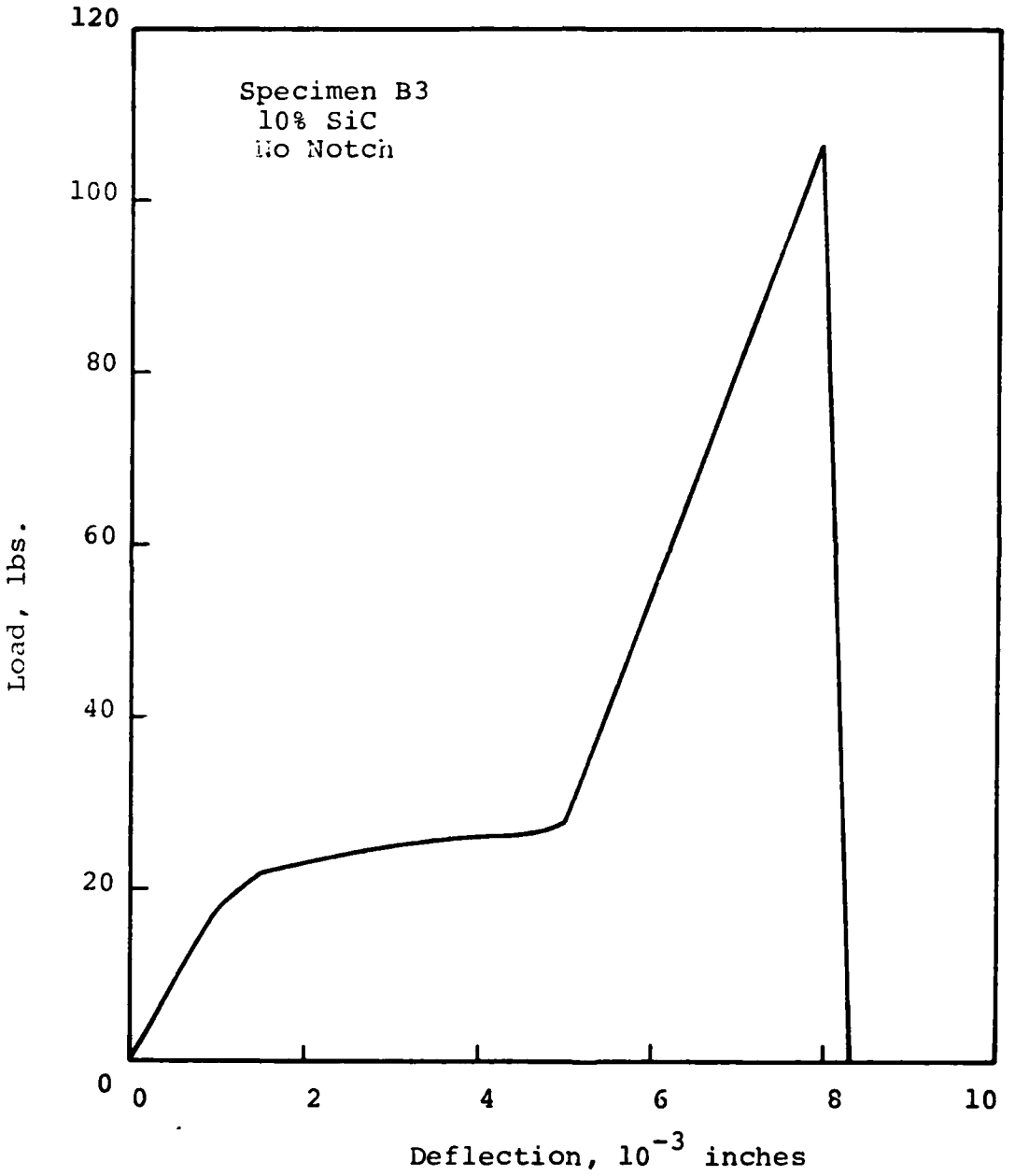

Figure 11. Load - Deflection response typical of SiC/Al_2O_3 composites with no notch

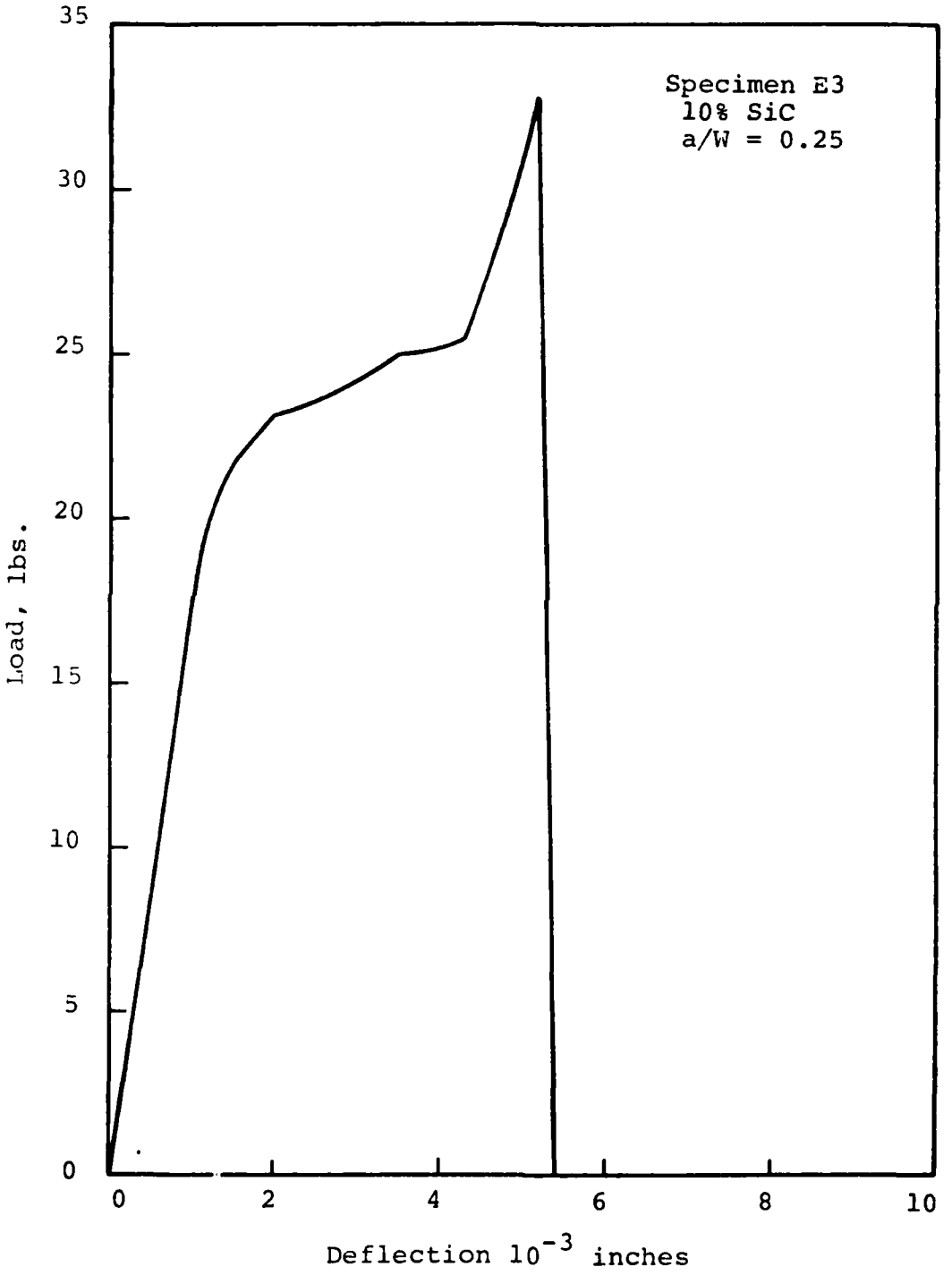

Figure 12. Load - Deflection response typical of SiC/Al_2O_3 composites with short and moderate notch length (a/W = 0.25 and 0.35)

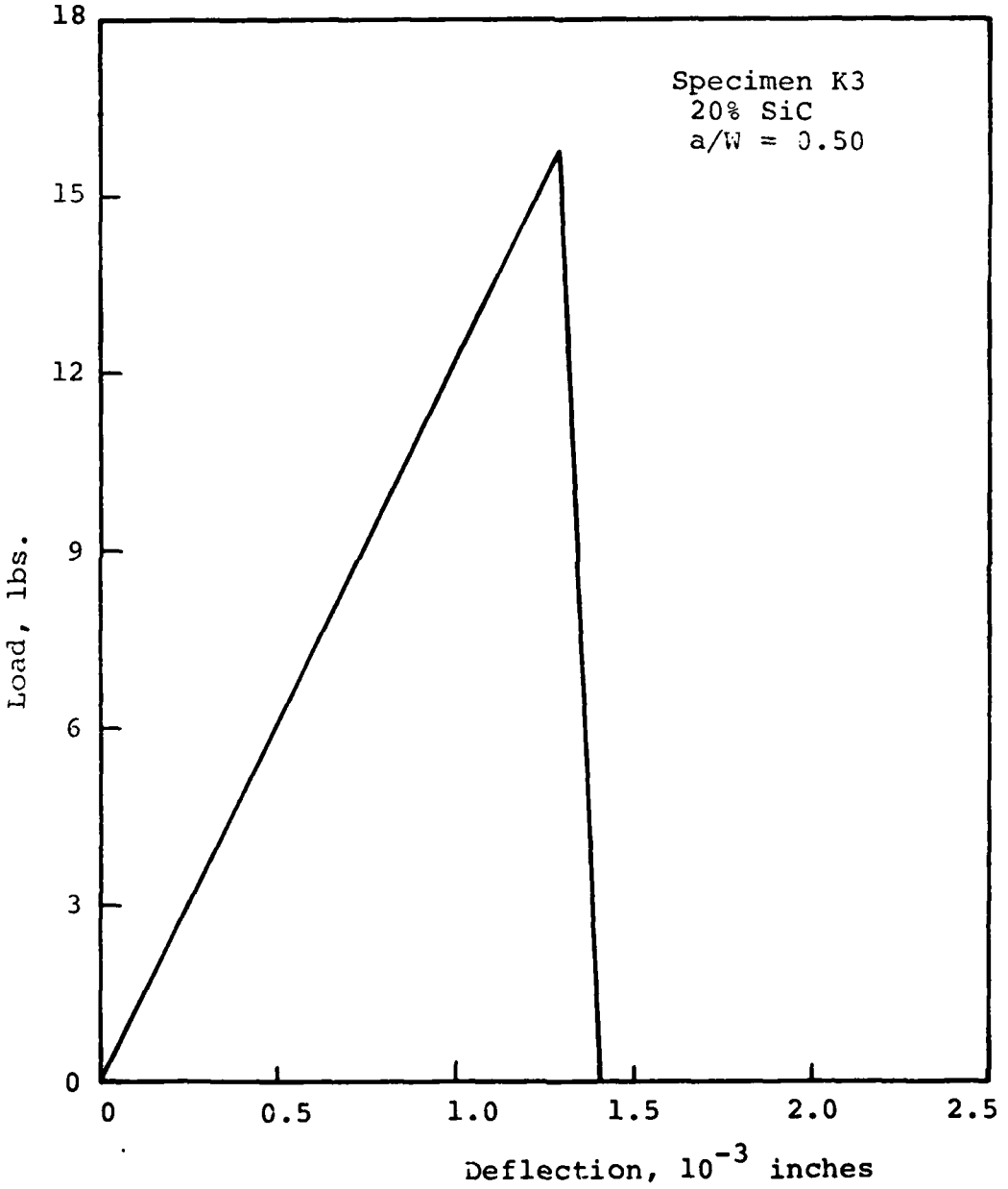

Figure 13. Load - Deflection response typical of SiC/Al_2O_3 composites with large notch length (a/W = 0.5)

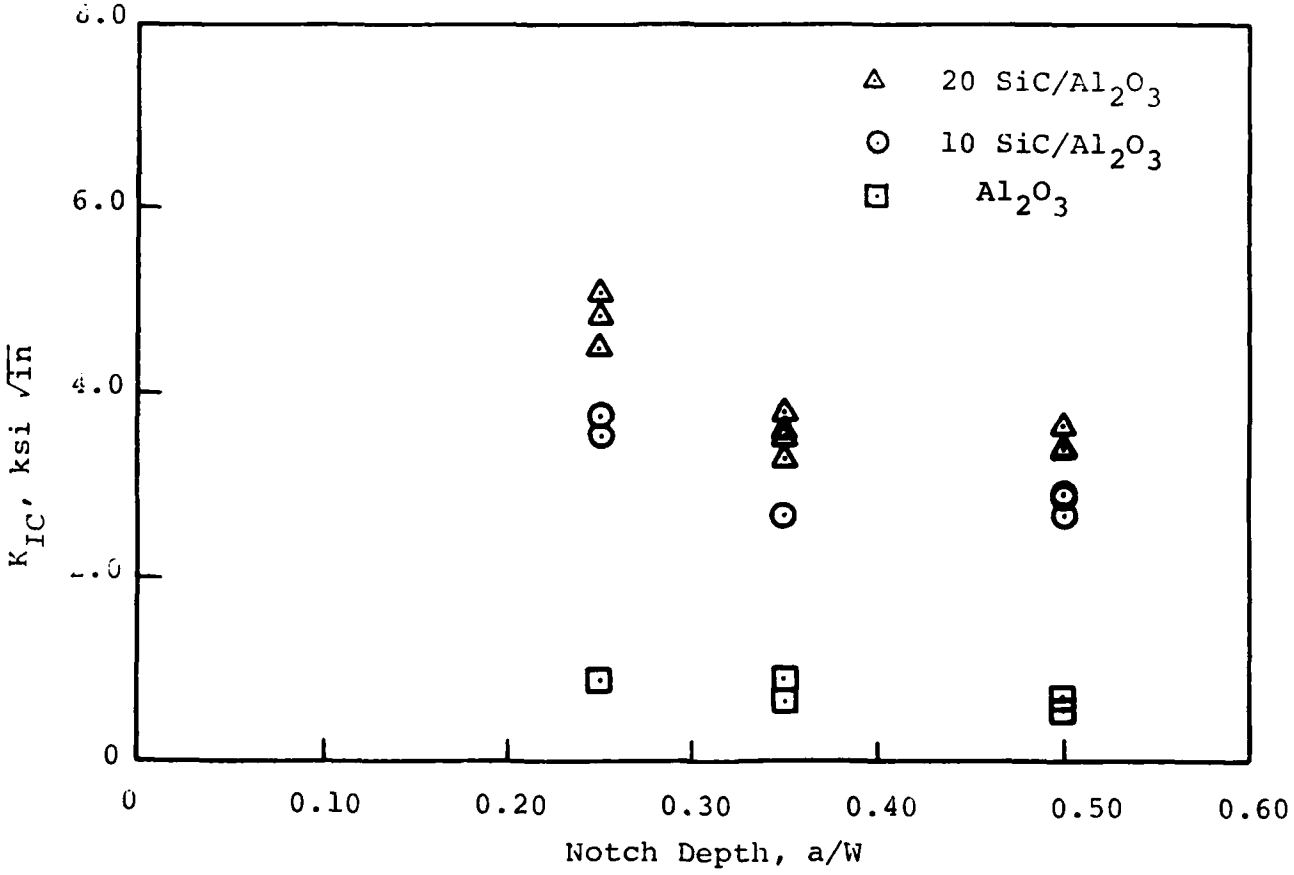

Figure 14. Measured Critical Stress Intensity Factor vs. Notch Depth for SiC/Al_2O_3 Composite Materials.

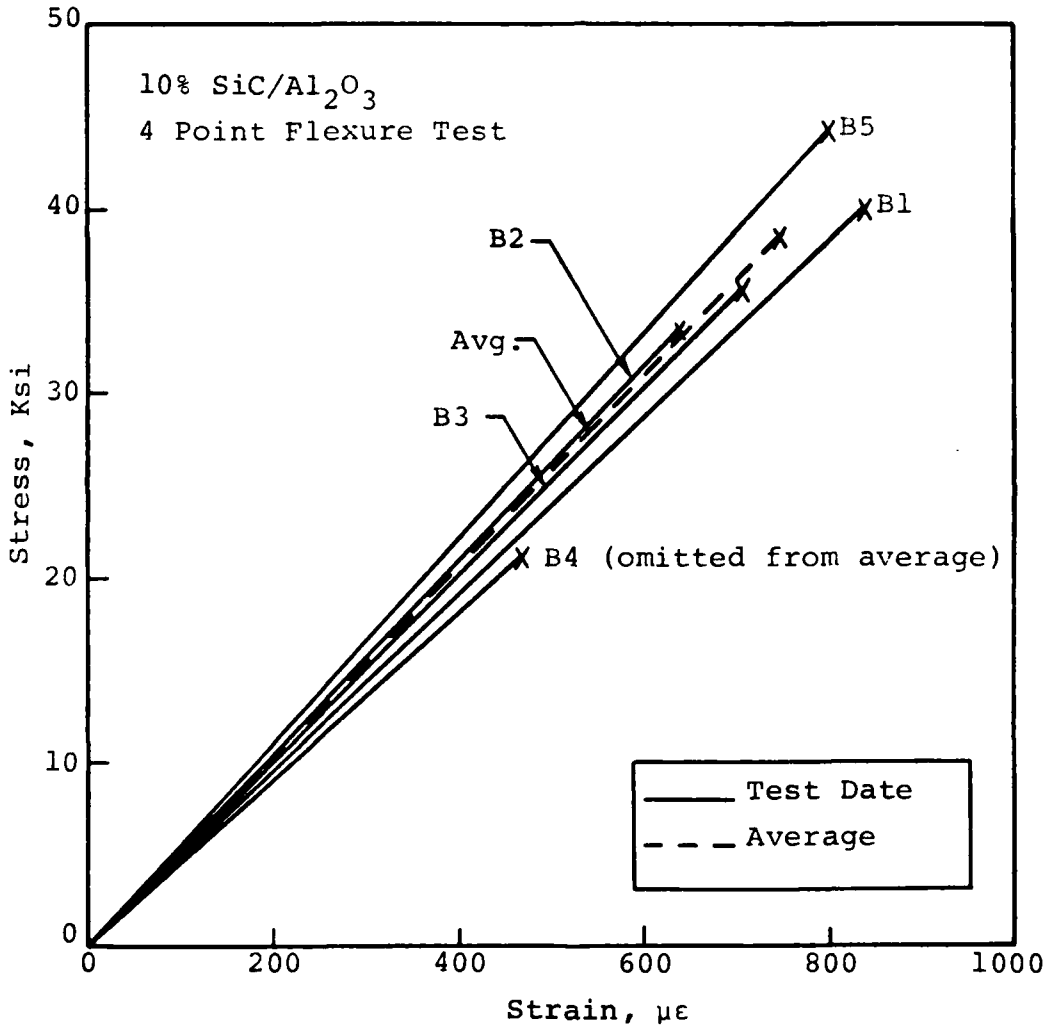

Figure 15. Measured Stress-Strain curves for SiC/Al_2O_3 Composites (10% SiC)

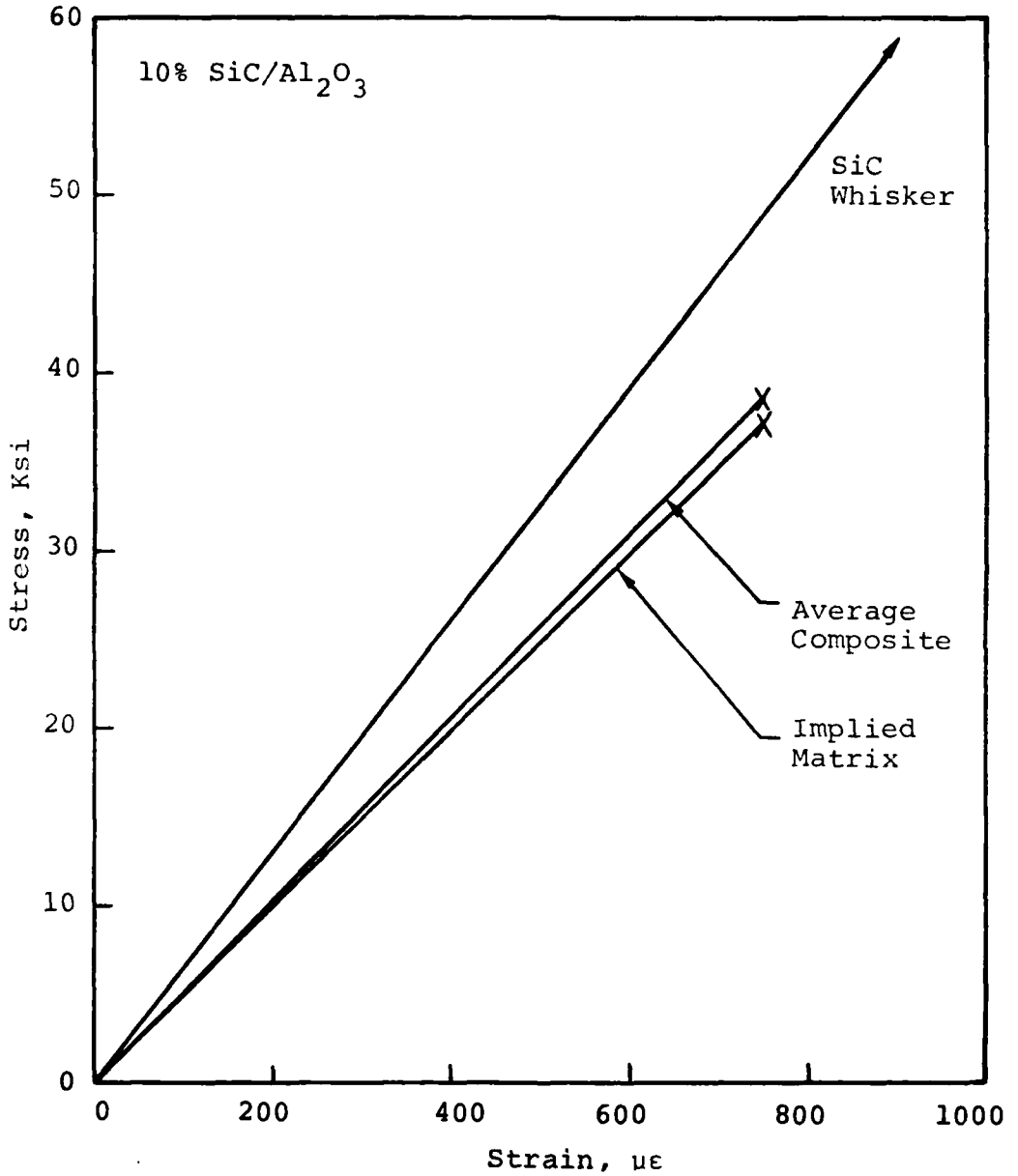

Figure 16. Comparison of Composite, Whisker and Matrix Stress-Strain curves for SiC/Al_2O_3 Composites (10% SiC)

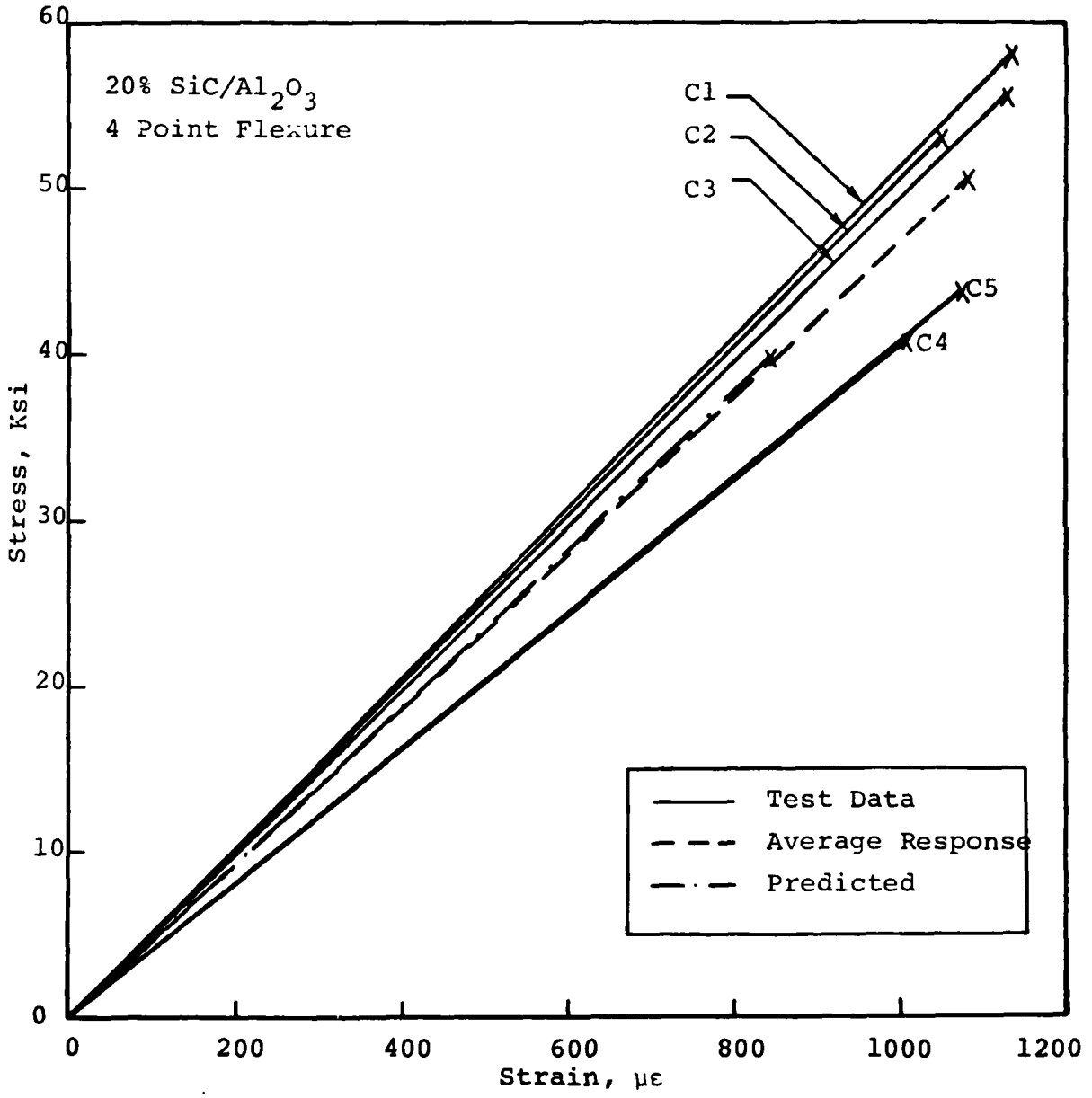

Figure 17. Measured Stress-Strain of SiC/Al_2O_3 composites (20% SiC). Figure shows comparison between measured 20% response and predicted 20% response which was based upon implied matrix properties.

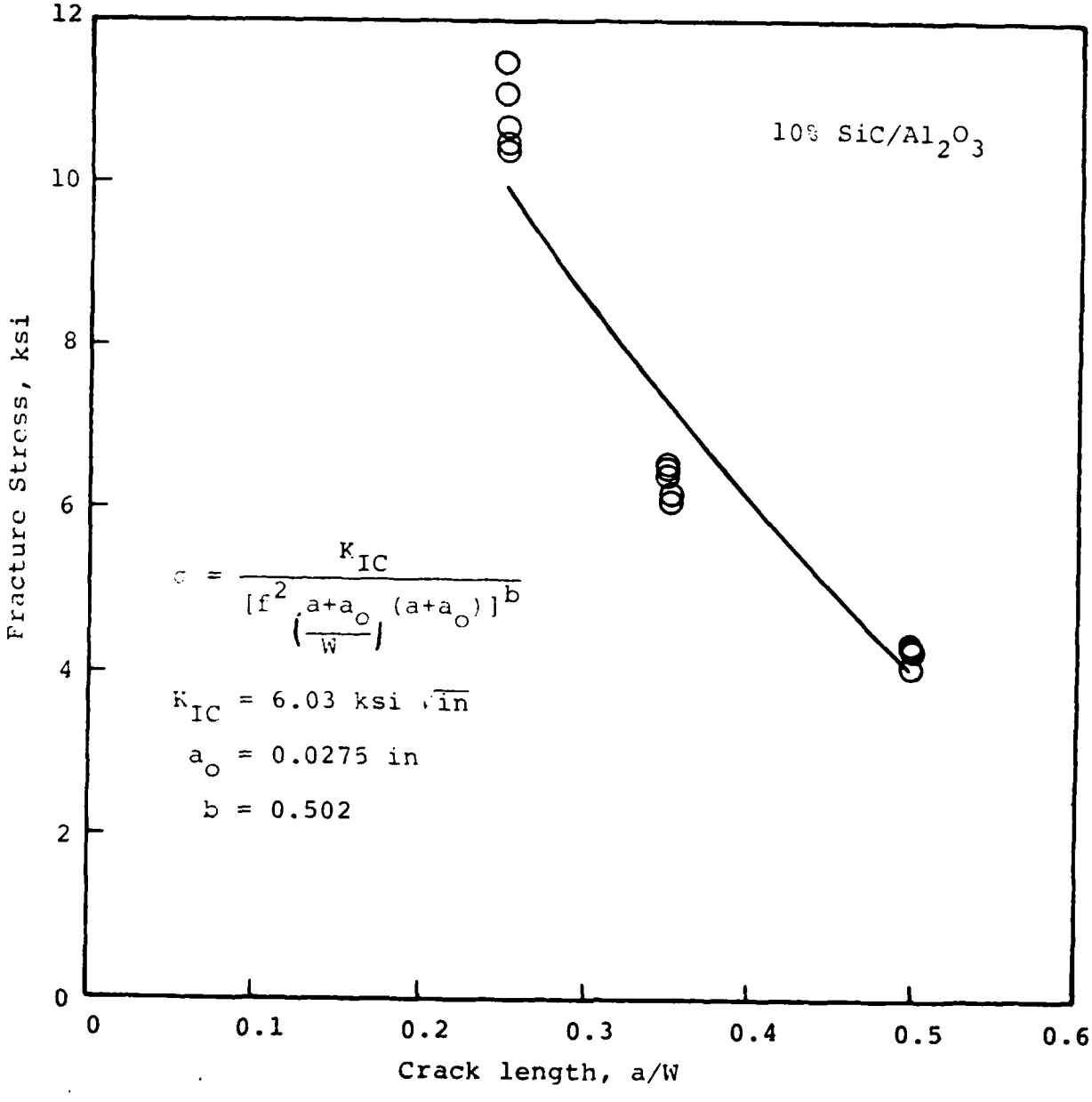

Figure 18. Curve fit of 10% SiC/Al_2O_3 Fracture Data Assuming Inherent Damage Zone. Results show that damage zone size and K_{IC} are unrealistically large.

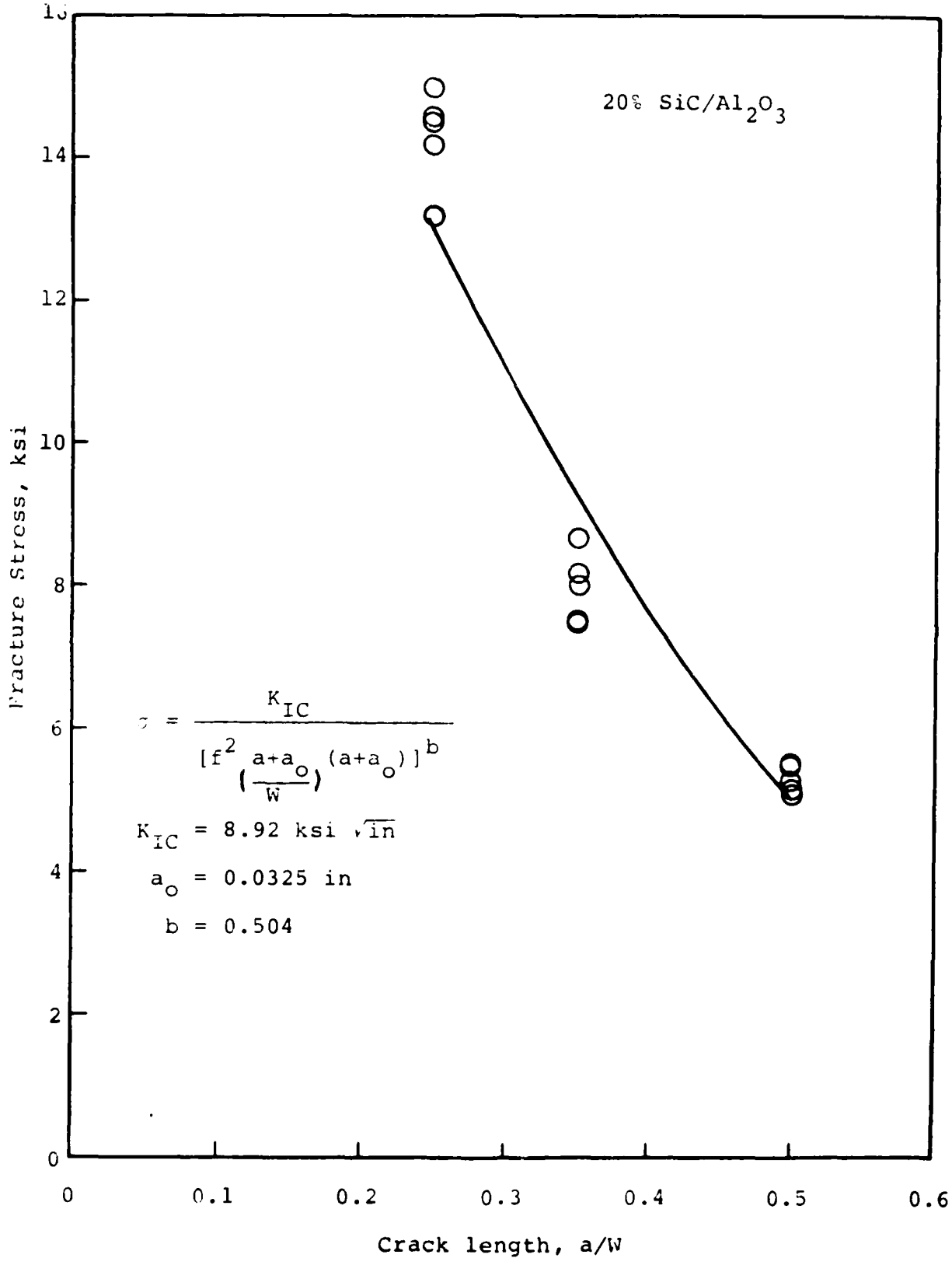

Figure 19. Curve fit of 10% SiC/Al_2O_3 Fracture Data Assuming Inherent Damage Zone. Results show that damage zone size and K_{IC} are unrealistically large.

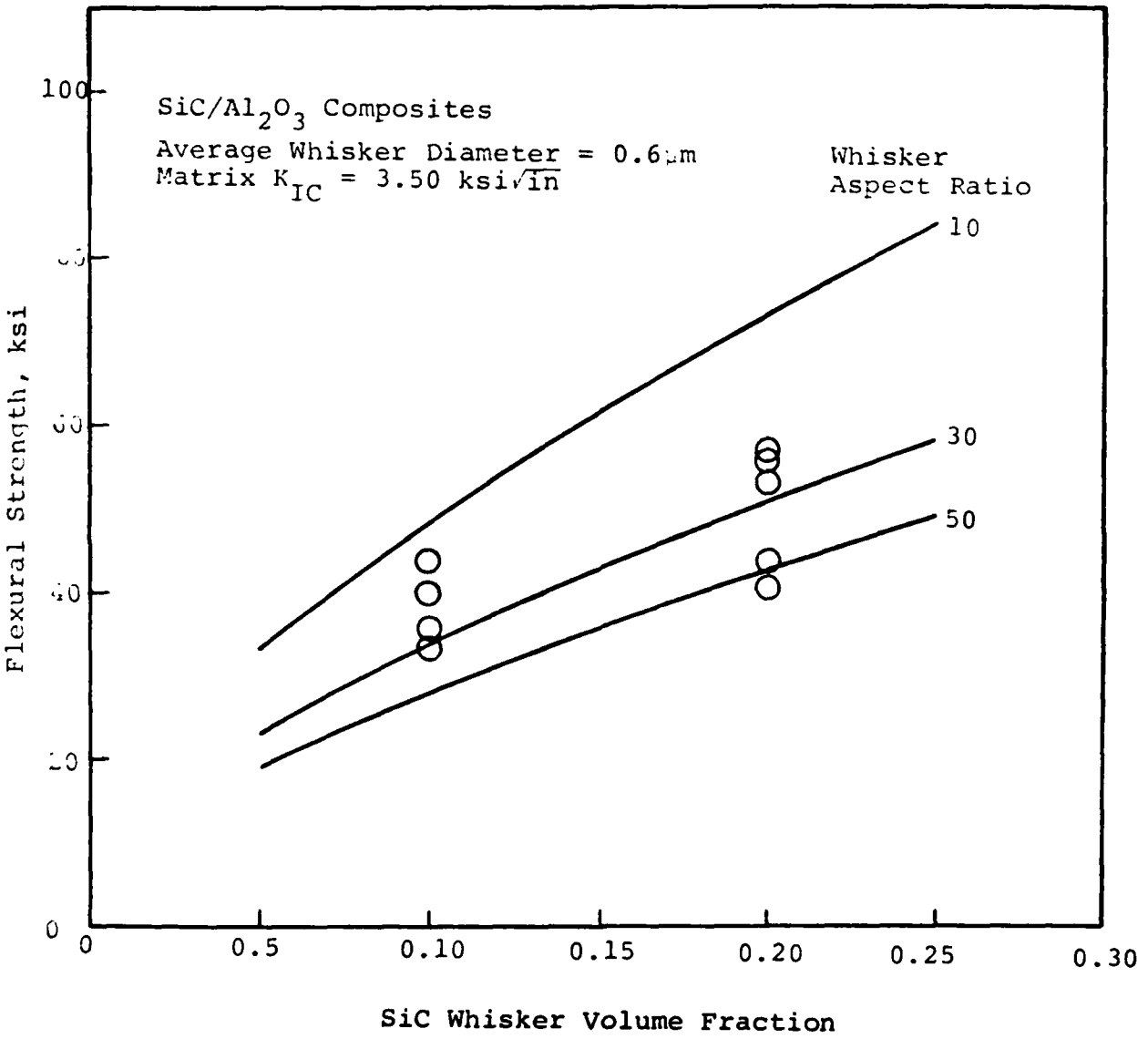

Figure 20. Comparison of Predicted vs. Measured Flexural Strength for SiC/Al2O3 Composites. Predictions based upon fracture of inherent flaw whose size is equal to the mean free path between whiskers.

APPENDIX - EXPERIMENTAL DATA

This appendix includes the measured experimental data, computed strengths, fracture toughnesses and SEM micrographs for the materials that were tested during this study.

Table A-1 shows the measured loads and deflections determined from the raw experimental data for each specimen. The table includes specimen number, SiC volume content, notch depth and measured data. The loads (column 4) and deflections (column 5) were chosen at a convenient point on the curves and were used to compute stiffness (column 6). The maximum load carried by the material is tabulated (column 7) along with the total deflection (column 8). Note that the total deflection includes the effects of fixture slippage which were discussed in the report. Therefore, these deflections can not be related to an ultimate material strain. Table A-2 presents the computed flexural strength obtained for the unnotched specimens. Table A-3 presents the computed critical stress intensities for the notched specimens. Figures A-1 through A-9 present SEM views of the notched specimens. The characteristics seen here are similar to those described previously. Each figure represents three views of a particular material and a particular notch depth.

Table A-1. Experimental Data on SiC/Al_2O_3 Materials

Specimen -	SiC v/o	Notch Depth a/W	P lbs	Δ^* 10^{-3} in	K^* 10^3 lb/in	Pmax lbs	Δ^* @ Pmax 10^{-3} in
A1	0	0	-	-	-	-	-
A2	0	0	8.50	1.14	7.46	12.8	2.68
A3	0	0	8.50	1.20	7.08	10.5	1.79
A4	0	0	5.50	0.77	7.14	10.7	3.76
A5	0	0	8.60	1.19	7.23	10.7	1.83
A6	0	0	10.0	1.30	7.69	10.5	1.70
A7	0	0	7.60	1.15	6.61	9.2	2.00
A8	0	0	10.0	1.23	8.13	10.8	1.50
A9	0	0	6.0	1.10	5.45	8.9	2.30
A10	0	0	5.8	1.15	5.04	8.2	2.15

*Crosshead Deflection

Table A-1. Experimental Data for SiC/Al_2O_3 Materials (con't)

Specimen -	SiC v/o	Notch Depth a/W	P lbs	Δ^* 10^{-3} in	K^* 10^3 lb/in	Pmax lbs	Δ^* @ Pmax 10^{-3} in
B1	10	0	119	4.70	25.3	119	9.80
B2	10	0	100	3.60	27.8	100	7.60
B3	10	0	107	4.0	26.8	107	7.95
B4	10	0	62.5	2.6	24.0	62.5	6.40
B5	10	0	131	4.5	29.1	131	8.40
C1	20	0	158	5.9	26.8	158	9.7
C2	20	0	173	6.35	27.2	173	10.6
C3	20	0	166	6.30	26.3	166	9.9
C4	20	0	121	5.65	21.4	121	9.5
C5	20	0	131	6.05	21.7	131	10.1

*Crosshead Deflections

Table A-1. Experimental Data on SiC/Al_2O_3 Materials (con't)

Specimen -	SiC v/o	Notch Depth a/W	P lbs	Δ^* 10^{-3} in	K^* 10^3 lb/in	Pmax lbs	Δ^* @ Pmax 10^{-3} in
D1	0	0.25	12.5	2.40	5.21	7.5	2.05
D2	0	0.25	7.5	1.03	7.28	9.25	1.42
D3	0	0.25	6.25	1.15	5.43	8.25	2.10
D4	0	0.25	6.5	1.05	6.19	8.0	1.50
D5	0	0.25	6.0	1.20	5.00	7.5	1.97
E1	10	0.25	17.25	1.05	16.4	30.9	5.22
E2	10	0.25	19.0	1.18	16.1	31.3	5.15
E3	10	0.25	20.0	1.27	15.7	32.9	5.23
E4	10	0.25	20.0	1.25	16.0	34.1	5.33
E5	10	0.25	20.0	1.29	15.5	31.5	5.02
F1	20	0.25	20.0	1.30	15.4	42.4	6.0
F2	20	0.25	20.0	1.30	15.4	39.2	5.85
F3	20	0.25	20.0	1.25	16.0	44.5	5.95
F4	20	0.25	17.5	1.17	15.0	43.5	5.45
F5	20	0.25	17.5	1.10	15.9	43.2	5.93

*Crosshead Deflections

Table A-1. Experimental Data for SiC/Al_2O_3 Materials (con't)

Specimen -	SiC v/o	Notch Depth a/W	P lbs	Δ^* 10^{-3} in	K^* 10^3 lb/in	Pmax lbs	Δ^* @ Pmax 10^{-3} in
G1	0	0.35	10	1.32	7.58	6.0	1.45
G2	0	0.35	5.0	0.95	5.26	5.5	1.40
G3	0	0.35	5.0	1.03	4.85	4.25	1.25
G4	0	0.35	5.0	0.97	5.15	4.70	1.25
G5	0	0.35	4.75	0.97	4.90	4.65	1.30
I1	10	0.35	15.0	1.25	12.0	18.2	2.22
I2	10	0.35	15.0	1.00	15.0	18.5	2.30
I3	10	0.35	15.0	1.02	14.7	19.3	2.80
I4	10	0.35	15.0	0.95	15.8	19.5	2.95
I5	10	0.35	15.0	1.05	14.3	19.2	2.85
H1	20	0.35	15.0	1.30	11.5	24.4	5.32
H2	20	0.35	15.0	1.25	12.0	23.8	5.52
H3	20	0.35	15.0	1.22	12.3	22.3	5.00
H4	20	0.35	15.0	1.25	12.0	25.8	5.55
H5	20	0.35	15.0	1.30	11.5	23.9	5.35

*Crosshead Deflections

Table A-1. Experimental Data on SiC/Al_2O_3 Materials (con't)

Specimen -	SiC v/o	Notch Depth a/W	P lbs	Δ^* 10^{-3} in	K^* 10^3 lb/in	Pmax lbs	Δ^* @ Pmax 10^{-3} in
J1	0	0.50	5.0	1.10	4.55	3.20	1.22
J2	0	0.50	10.0	2.25	4.44	3.15	1.0
J3	0	0.50	10.0	1.95	5.13	3.30	0.97
J4	0	0.50	10.0	1.95	5.13	2.50	1.45
J5	0	0.50	10.0	3.15	3.17	2.50	1.15
L1	10	0.50	12.95	1.0	13.0	12.95	1.0
L2	10	0.50	12.15	0.97	12.5	12.15	0.97
L3	10	0.50	12.15	1.07	11.4	12.15	1.07
L4	10	0.50	13.1	1.0	13.1	13.1	1.0
L5	10	0.50	12.8	1.0	12.8	12.8	1.0
K1	20	0.50	15.0	1.37	10.9	16.3	1.65
K2	20	0.50	15.0	1.30	11.5	15.25	1.40
K3	20	0.50	15.75	1.25	12.6	15.75	1.25
K4	20	0.50	16.05	1.27	12.6	16.3	1.27
K5	20	0.50	15.35	1.20	12.8	15.35	1.20

*Crosshead Deflections

Table A-2. Measured Flexural Strength of SiC/Al_2O_3 Materials

Specimen -	SiC v/o	Notch Depth a/W	Pmax lbx	σ_b^{alt} Ksi
A1	0	0	-	-
A2	0	0	12.8	4.30
A3	0	0	10.5	3.53
A4	0	0	10.7	3.60
A5	0	0	10.7	3.60
A6	0	0	10.5	3.53
A7	0	0	9.2	3.09
A8	0	0	10.8	3.63
A9	0	0	8.9	2.99
A10	0	0	8.2	2.76

Table A-2. Measured Flexural Strength of SiC/Al_2O_3 Materials (con't)

Specimen -	SiC v/o	Notch Depth a/W	Pmax lbs	σ_b^{alt} Ksi
B1	10	0	119	40.0
B2	10	0	100	33.6
B3	10	0	107	36.0
B4	10	0	62.5	21.0
B5	10	0	131	44.0
C1	20	0	158	53.1
C2	20	0	173	58.1
C3	20	0	166	55.8
C4	20	0	121	40.7
C5	20	0	131	44.0

Table A-3. Measured Stress Intensity Factors for SiC/Al_2O_3 Materials

Specimen -	SiC v/o	Notch Depth a/W	Pmax lbs	K_{Ic} Ksi $\sqrt{in}$
D1	0	0.25	7.5	0.86
D2	0	0.25	9.25	1.06
D3	0	0.25	8.25	0.94
D4	0	0.25	8.0	0.91
D5	0	0.25	7.5	0.86
E1	10	0.25	30.9	3.53
E2	10	0.25	31.3	3.57
E3	10	0.25	32.9	3.75
E4	10	0.25	34.1	3.89
E5	10	0.25	31.5	3.59
F1	20	0.25	42.4	4.84
F2	20	0.25	39.2	4.47
F3	20	0.25	44.5	5.08
F4	20	0.25	43.5	4.96
F5	20	0.25	43.2	4.93

Table A-3. Measured Stress Intensity Factors for SiC/Al_2O_3 Materials (con't)

Specimen -	SiC v/o	Notch Depth a/W	Pmax lbs	K_{Ic} Ksi $\sqrt{in}$
G1	0	0.35	6.0	0.88
G2	0	0.35	5.5	0.81
G3	0	0.35	4.25	0.63
G4	0	0.35	4.70	0.69
G5	0	0.35	4.65	0.69
I1	10	0.35	18.2	2.68
I2	10	0.35	18.5	2.72
I3	10	0.35	19.3	2.84
I4	10	0.35	19.5	2.87
I5	10	0.35	19.2	2.83
H1	20	0.35	24.4	3.59
H2	20	0.35	23.8	3.51
H3	20	0.35	22.3	3.28
H4	20	0.35	25.8	3.80
H5	20	0.35	23.9	3.52

Table A-3. Measured Stress Intensity Factors for SiC/Al_2O_3 Materials (con't)

Specimen -	SiC v/o	Notch Depth a/w	Pmax lbs	K_{Ic} Ksi $\sqrt{in}$
J1	0	0.50	3.20	0.71
J2	0	0.50	3.15	0.70
J3	0	0.50	3.30	0.74
J4	0	0.50	2.50	0.56
J5	0	0.50	2.50	0.56
L1	10	0.50	12.95	2.89
L2	10	0.50	12.15	2.71
L3	10	0.50	12.15	2.71
L4	10	0.50	13.1	2.92
L5	10	0.50	12.8	2.85
K1	20	0.50	16.3	3.63
K2	20	0.50	15.25	3.40
K3	20	0.50	15.75	3.51
K4	20	0.50	16.3	3.63
K5	20	0.50	15.35	3.42

15X

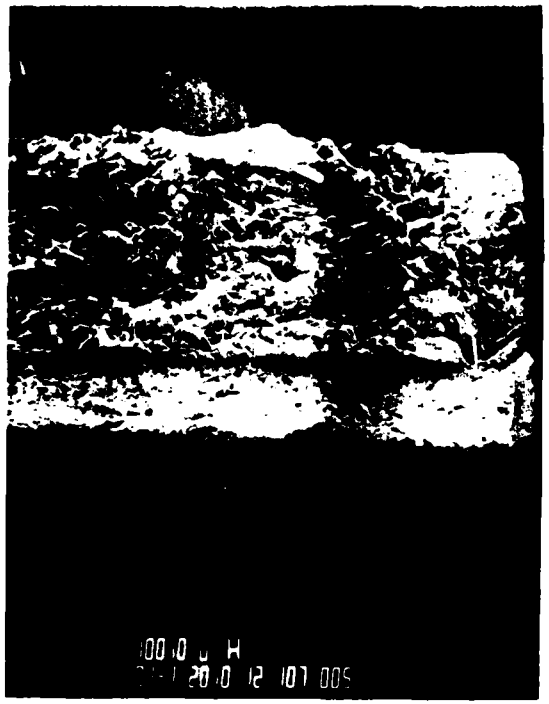

50X

500X

Figure A-1. Fracture Surface of SiC/Al_2O_3 Composite (0% SiC, a/W=0.25)

2500X

5000X

10,000X

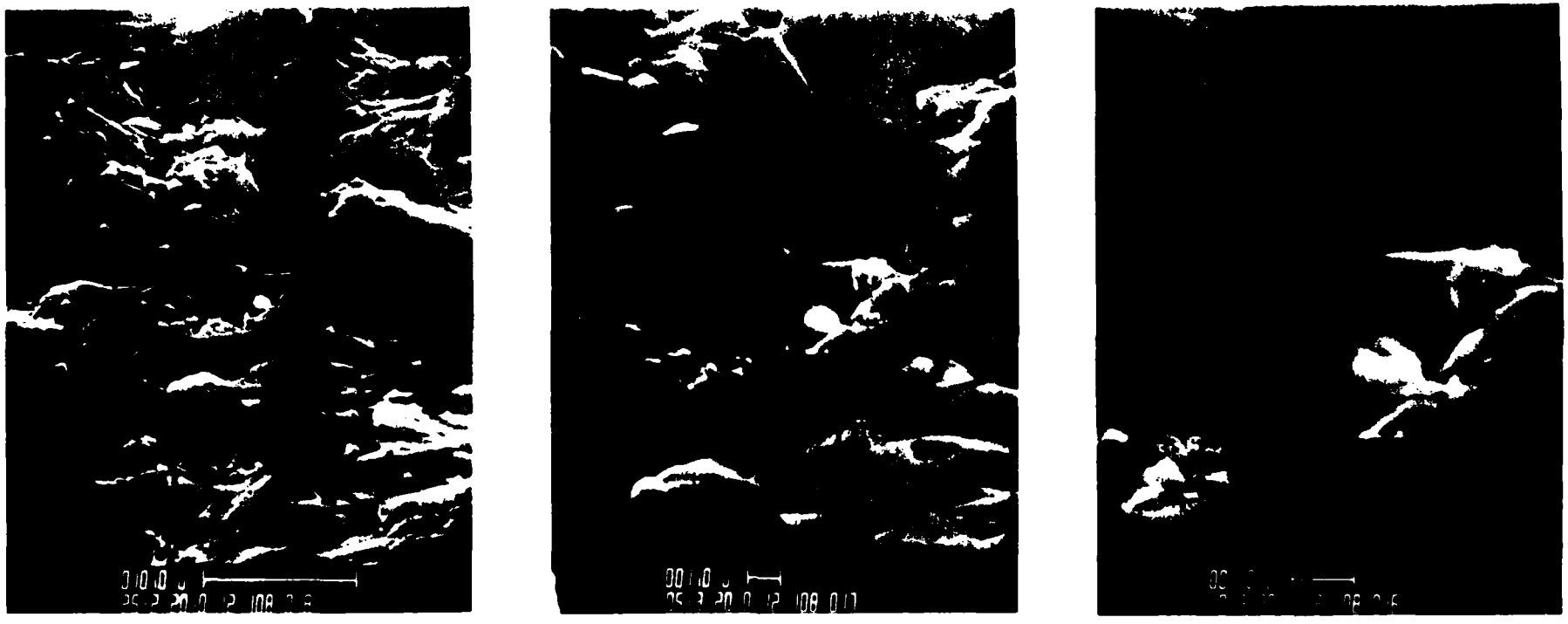

Figure A-2. Fracture Surface of SiC/Al_2O_3 Composite (10% Sic, a/W=0.25)

2500X

5000X

10,000X

Figure A-3. Fracture Surface of SiC/Al_2O_3 Composite (20% SiC, a/W=0.25)

15X

50X

250X

Figure A-4. Fracture Surface of SiC/Al_2O_3 Composite (0% SiC, a/W=0.375)

2500X

5000X

10,000X

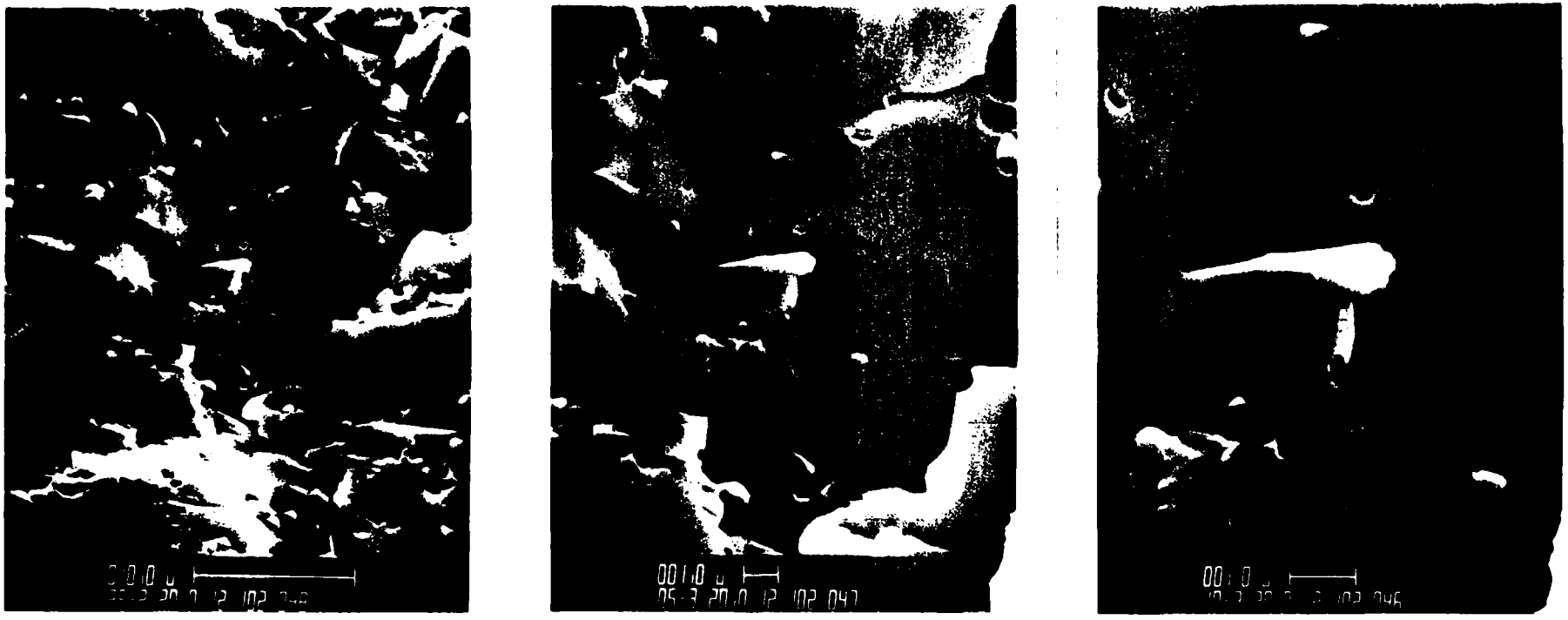

Figure A-5. Fracture Surface of SiC/Al_2O_3 Composite (10% SiC, a/W=0.375)

2500X

5000X

10,000X

Figure A-6. Fracture Surface of SiC/Al_2O_3 Composite (20% SiC, a/W=0.375)

25X

200X

1000X

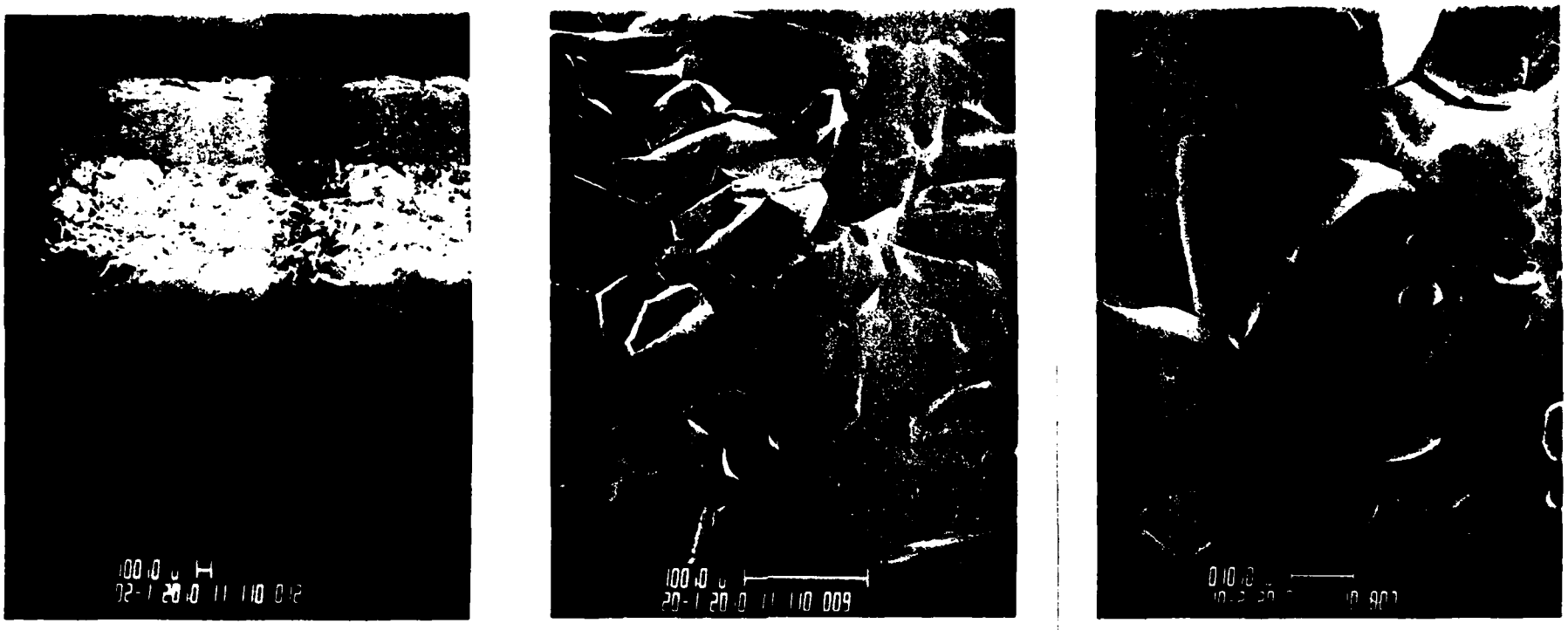

Figure A-7. Fracture Surface of SiC/Al_2O_3 Composite (0% SiC, a/W=0.5)

2500X

5000X

10,000X

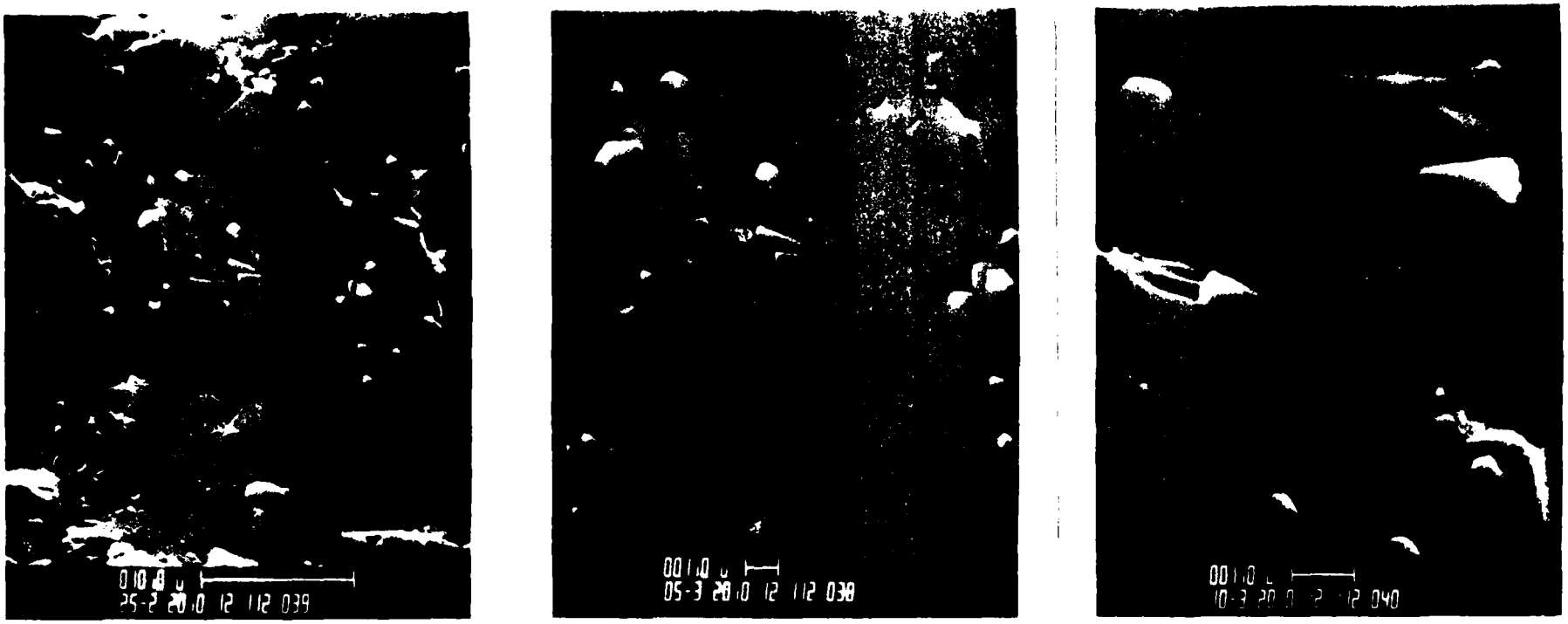

Figure A-8. Fracture Surface of SiC/Al_2O_3 Composite
(10% SiC, a/W=0.5)

2500X

5000X

10,000X

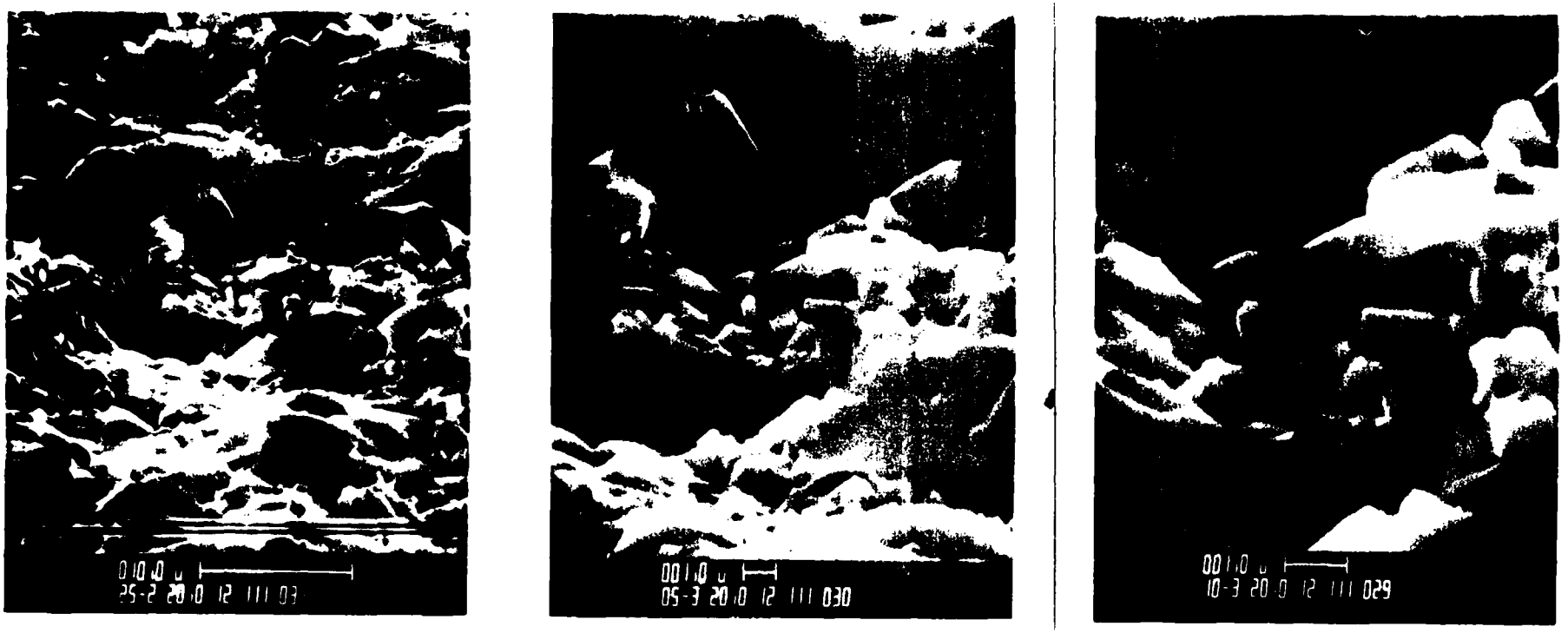

Figure A-9. Fracture Surface of SiC/Al_2O_3 Composite (20% SiC, a/W=0.5)

END

FILMED

3-85

DTIC